ATMOSPHERIC SCIENCE ON THE GALILEO MISSION*

D. M. HUNTEN

Lunar and Planetary Laboratory, The University of Arizona, U.S.A.

L. COLIN

NASA-Ames Research Center, U.S.A.

and

J. E. HANSEN

NASA-Goddard Institute for Space Studies, U.S.A.

(Received 26 November, 1986)

Table of Contents

Abstract. Observations from the ground and four fly-by spacecraft have provided initial reconnaissance of Jupiter's atmosphere. The Pioneer and Voyager data have raised new questions and underlined old ones about the basic state of the atmosphere and the processes determining the atmosphere's behavior. This paper discusses the main atmospheric science objectives which will be addressed by the Galileo (Orbiter

* The Atmospheres Working Group also includes: M. D. Allison, M. J. S. Belton, R. W. Boese, R. W. Carlson, C. R. Chapman, T. Encrenaz, V. R. Eshleman, P. J. Gierasch, C. W. Hord, H. T. Howard, L. J. Lanzerotti, H. B. Niemann, G. S. Orton, T. Owen, C. B. Pilcher, J. B. Pollack, B. Ragent, W. B. Rossow, A. Seiff, A. I. Stewart, P. H. Stone, F. W. Taylor, G. L. Tyler, U. von Zahn, and R. A. West.

Space Science Reviews **44** (1986) 191–240.

and Probe) mission, organizing the discussion according to the required measurements of chemical composition, thermal structure, clouds, radiation budget, dynamics, upper atmosphere, and satellite atmospheres. Progress on the key questions will contribute not only to our knowledge of Jupiter's atmosphere but to a general understanding of atmospheric processes which will be valuable for helping us to understand the atmosphere and climate of the Earth.

Realization of the atmospheric science objectives of the Galileo mission depends upon: (a) coordinated measurements from the entry probe and the orbiter; (b) global observations; and (c) observations over the range of time-scales needed to characterize the basic dynamical processes.

1. Introduction

This review describes the objectives of the Galileo mission for improving our understanding of the Jovian atmosphere, and the investigations that contribute. The first-order atmospheric objectives are to determine (1) the chemical composition of the atmosphere, (2) the thermal structure of the atmosphere, (3) the nature of cloud particles and cloud layering, (4) the radiative energy balance, and to investigate (5) atmospheric dynamics and (6) the upper atmosphere. The capability of Galileo to explore the tenuous atmospheres of the satellites is briefly discussed.

Powerful remote-sensing techniques have been applied to Jupiter's atmosphere from Pioneers 10 and 11, Voyagers 1 and 2, and the Earth. Remote sensing will also be carried out from the Galileo Orbiter, but the truly new aspect is the entry probe, which will make direct measurements from $\sim 10^{-10}$ bar to 10–20 bars, although only one instrument is activated prior to the 100 mb level. The entry trajectory is summarized on the temperature profile in Figure 6. Engineering specifications on the Probe and its experiments guarantee, insofar as possible, measurements and communications to at least 10 bars. The designs of the hardware and of the radio link give an expected yield to 20–25 bars. Most remote measurements from the orbiter will pertain to a rather poorly-defined level around 600 mb. Table I lists the Probe and relevant Orbiter experiments with their acronyms. Further details are given in Section 3. Section 2 discusses the current state

TABLE I

Galileo instruments with atmospheric objectives

Instrument[a]	Abbreviation
Atmospheric structure instrument (P)	ASI
Neutral mass spectrometer (P)	NMS
Helium abundance interferometer (P)	HAD or HAI
Nephelometer (P)	NEP
Net flux radiometer (P)	NFR
Lightning and radio emission detector (P)	LRD
Solid state imaging system (O)	SSI
Near infrared mapping spectrometer (O)	NIMS
Photopolarimeter – radiometer (O)	PPR
Ultraviolet spectrometer (O)	UVS
Radio science (O, P)	RS

[a] (P): on Probe; (O): on Orbiter.

of knowledge and the expected contributions of the Galileo mission toward improving that knowledge; the approach is to focus on major questions, rather than attempt to be exhaustive.

2. Present Knowledge of Jupiter's Atmosphere and Key Questions for the Galileo Mission

2.1. Chemical composition

Jupiter's atmospheric composition and bulk properties (especially the mean density) are generally consistent with the idea that the overall elemental composition is similar to that of the Sun. There is a dense core with a mass of some 30 Earth masses, or 10% of Jupiter's mass. Undoubtedly it contains 'rocky' materials, chiefly iron and silicates. The principal remaining substances can be classified as 'ices' (H_2O, NH_3, CH_4) and the gases H_2 and He. If the ices (or even helium) were accreted to the core before the atmosphere formed, they would remain there because of the large density contrast. Conversely, as gases or vapors they would remain in the atmosphere if they were present there originally; only condensed drops or particles can sink at a significant rate. It is therefore impossible to say *a priori* what fraction of the vapors would be expected in the observable atmosphere. The observed amounts of helium, methane, and ammonia are close to those expected for solar composition; that of water vapor is much lower. It is conceivable that most of the H_2O is gravitationally trapped on or near the core.

Segregation of hydrogen and helium is very unlikely under Jovian conditions. The escape time for H_2 molecules from the atmosphere is much longer than the age of the Universe. Jupiter is expected to be the best place to measure the solar abundance of helium. Otherwise, the relative proportions of the molecular constituents of Jupiter are important for establishing conditions at the time of planetary formation, and they provide a point of comparison with the other planets which is crucial to the task of unraveling the origin and evolution of the entire planetary system. Molecular abundances and their variations with altitude are also important for studying Jovian cloud physics and atmospheric chemistry.

Of necessity, all the existing information on composition is derived from remote sensing. Analysis of such data typically gives results with small random errors but unknown systematic errors. With direct sensing these systematic errors can be, and usually are, included in an overall error estimate. The quoted error numbers may be similar, or even larger, but they are more realistic. For many substances (particularly NH_3 and H_2O) the calibration errors may dominate, and are common to all methods.

Available data suggest that hydrogen and helium in Jupiter's atmosphere are close to their proportions in the solar atmosphere, where the helium volume fraction $[He]/([H_2] + [He])$ is approximately 0.112 (Ross and Aller, 1976). Analysis of Voyager infrared spectroscopy in the range 280–600 cm^{-1} yields a volume fraction of 0.11 ± 0.03 for He (Hanel *et al.*, 1979a,b; Gautier *et al.*, 1981), in good agreement with the previous estimate of 0.12 ± 0.06 from Pioneer spacecraft observations (Orton and

Ingersoll, 1976). The Saturn value is lower by several percent. The Helium Abundance Interferometer on the Galileo Probe is expected to obtain the helium volume fraction with an uncertainty of 0.001 in the 2.5–10 bar region, providing an improvement of 30 times in accuracy compared to the Voyager data. The Probe Neutral Mass Spectrometer will also measure the helium volume fraction, with an estimated uncertainly of 0.01, for depths from about 100 mb to at least 10 bars.

The ratio of deuterium to hydrogen is also of cosmogenical significance. Reeves *et al.* (1973) argued that 'big bang' nucleosynthesis is the only viable production mechanism and that nuclear burning to produce ^{3}He is an efficient loss mechanism; the Jovian D/H ratio is generally assumed to be indicative of the primordial value (see Gautier and Owen, 1983a,b). Current estimates of D/H on Jupiter range at least from 1.8×10^{-5} (Drossart *et al.*, 1982) to $5.1 \pm 0.7 \times 10^{-5}$ (Trauger *et al.*, 1977), the former value being consistent with local interstellar values while the latter suggests substantial enrichment. The Voyager value is $(1.9-4.1) \times 10^{-5}$ (Kunde *et al.*, 1982). The analysis by Bjoraker *et al.* (1986a), which combines data from Voyager and airborne instruments (with higher spectral resolution) gives $(1.2 \pm 0.5) \times 10^{-5}$. This paper contains useful summaries of earlier work. Measurements by the NMS on the Galileo Probe should resolve the uncertainty.

Molecular hydrogen exists in two essentially non-interchangeable forms; *para*-H_2 (even rotational levels) and *ortho*-H_2 (odd rotational levels). The slow rate of conversion makes the *o/p* ratio of interest as a tracer for atmospheric motions. Conrath and Gierasch (1984) have found from Voyager data large departures from the ratio expected at the local temperature, implying that the gas at $\sim$200 mb was recently at a much greater pressure level. The Galileo Photopolarimeter Radiometer (PPR) experiment, as well as ground-based observations, may be able to pursue this matter.

Methane (CH_4) should contain most of the C on Jupiter and thus permit determination of how the C/H ratio in the atmosphere of Jupiter compares to that in the atmosphere of the Sun. The most detailed analysis of ground-based observations of both weak and strong CH_4 absorption bands in the spectra of solar radiation reflected by Jupiter yields $(1.8 \pm 0.4) \times 10^{-3}$ for $[CH_4]/[H_2]$ (Sato and Hansen, 1979), corresponding to 2.0 ± 0.4 times the current estimates for the abundance of C in the atmosphere of the Sun. Other analyses of CH_4 bands in reflected solar light have yielded C/H ratios between 3.2–3.6 times the solar value (Buriez and de Bergh, 1980; Bjoraker *et al.* (1986a)) and 2 times the solar value (Encrenaz and Combes, 1982). (The still higher values discussed by Wallace and Hunten (1978) are a result of a smaller assumed value for the Sun.) The C/H value derived from observations in the infrared is also twice the solar value (Gautier *et al.*, 1982). Such variations illustrate the problems inherent in remote sensing; little progress can be expected until the Galileo NMS makes its direct measurements. These will serve as reference for the Orbiter and for future Earth-based measurements, whose usefulness will then be in determination of cloud structure. With the spectrophotometry of the NIMS experiment and the PPR polarimetry and photometry, observations in methane bands will allow the Galileo Orbiter to measure cloud heights (pressure levels) and the vertical structure of cloud layers. The high-resolu-

tion imaging system (SSI) on the Orbiter also includes two filters in CH_4 bands; thus, with the aid of coordinated analyses of the different measurements, it should be possible to extend some information on vertical cloud structure to the full resolution of the imaging system.

The N/H ratio and the vertical profile of major nitrogen compounds are also of fundamental importance. Central to this is the abundance of ammonia (NH_3), which probably exhibits substantial variability throughout the atmosphere of Jupiter because of such processes as photochemistry in the upper atmosphere, condensation at temperatures below approximately 145 K (Figure 1), dissolution in water clouds at depths of several bars, and chemical reaction with H_2S to form NH_4SH. Analysis of weak NH_3

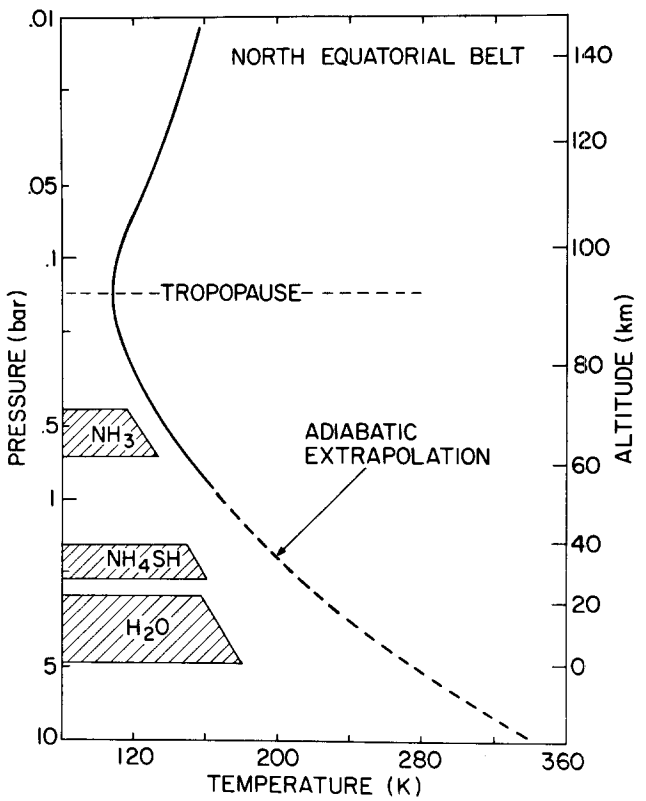

Fig. 1. Temperature structure for the NEB. The solid line represents the temperature profile obtained by inversion of the Voyager IRIS spectral radiances. The dashed line is an extrapolation from 0.8 bar to deeper levels along a 2.0 K km^{-1} adiabat. The theoretical cloud layers of Weidenschilling and Lewis (1973) are indicated schematically on the left (Kunde *et al.*, 1982).

bands in regions of the spectrum where the Jovian atmosphere is relatively transparent indicates that the NH_3 abundance is $(2.8 \pm 1.0) \times 10^{-4}$ for $[NH_3]/[H_2]$ in the 1–3 bar region just beneath the main visible cloud layer (Sato and Hansen, 1979), corresponding to 1.5 ± 0.5 times current estimates for the solar N/H ratio. From the analysis of 1100–1200 cm^{-1} spectra, Knacke *et al.* (1982) find an NH_3 abundance of

$(3.3 \pm 1.7) \times 10^{-4}$ below the 600 mb level. In the Voyager data, the 180–300 cm^{-1} region yields a value within a factor 2 of solar, 1.78×10^{-4} (Kunde *et al.*, 1982) or 2.6×10^{-4} in the re-analysis of Bjoraker *et al.* (1986a). At higher levels the depletion is very large, as clearly seen from the weakness of absorption around 2200 Å. At and below the 3-bar level, the centimeter-band thermal emission indicates an enhancement over solar by perhaps a factor of 2 (Gulkis and Poynter, 1972) or even more (Marten *et al.*, 1980). The same opacity, seen as absorption in the Voyager 1 radio occultations, gives a mole fraction of 2.2×10^{-4} at 1 bar, with rapid falloff to higher altitudes (Lindal *et al.*, 1981).

The NMS on the Galileo Probe will measure the NH_3 abundance over the height range 0.1–10 bars or deeper, unless the ammonia is depleted below the ppm level at the higher altitudes. The accuracy is likely to be limited by calibration errors to about 10%. Orbiter experiments will extend the coverage to the rest of the globe, but in a limited range of height. The PPR uses the 6450 Å band which pertains to pressures around 1 bar, as well as the region beyond 40 μm. The Near-Infrared Mapping Spectrometer (NIMS) makes use of several bands. The Ultraviolet Spectrometer (UVS) will be sensitive to NH_3 at altitudes above the ammonia cloud. Radio Science has the same potential as on Voyager, but few occultation opportunities will occur because of other constraints on the orbital geometry.

Water vapor and water clouds offer some of the most puzzling problems. Models of the origin and of the interior structure suggest that the bulk water content might exceed the solar value, about 10^{-3} or 1000 ppm (e.g., Cameron and Pollack, 1976). Remote observations are possible only in the special areas ('hot spots') that are clear of clouds to pressures of several bars. Kunde *et al.* (1982) find mixing ratios of 1 ppm at 2.5 bars and 30 ppm at 4 bars, each within a factor of 2. Earlier aircraft-based results are comparable (Larson *et al.*, 1974; Bjoraker *et al.*, 1981), and the combined analysis of Bjoraker *et al.* (1986b) gives 4 ppm in the 2–4 bar range, rising to 30 ppm at 6 bars. These results are not restricted to hot spots. Undoubtedly the hot spots are regions of subsidence, drier than average, but it is hard to imagine that they could be drier by the required factor of 30–1000. One of the primary purposes of the probe and some of its instruments is to resolve these questions by measuring H_2O in a region more representative than a hot spot, and to depths well below the condensation level, shown in Figure 1 as just less than 5 bars. A safety factor of 2 determines the engineering requirement of 10 bars on the Probe mission, and much deeper penetration is desired and expected.

Although a mass spectrometer can readily measure the H_2O in its ion source, it is a difficult problem to assure that this gas has not been altered on its way in, by adsorption of H_2O on the walls of the inlet system. Similar problems arise in laboratory calibration. Currently it is felt that an absolute accuracy of a factor of 2 is feasible, and possibly better. An *in situ* cross check may be available from measurement of the temperature at the condensation level, making use of the Atmospheric Structure Instrument and the Nephelometer. Another independent measurement will be made by the Net Flux Radiometer, one of whose infrared channels is occupied by a strong H_2O band. A large H_2O opacity will force the net flux into other wavelength regions and give

a low reading in this band. Such a measurement is free of sampling errors since it pertains to the ambient atmosphere.

Remote observation of H_2O is at best limited to hot spots, which can be observed in the 5 μm region; another band, at 2.7 μm, is within the NIMS capability and may be useful.

Phosphine, PH_3, was observed first from Earth, then by Voyager, at 5 and 9 μm; the two bands probe regions around 2 and 0.5 bar. Kunde *et al.* (1982) summarize these results (their Figure 17), which indicate a mixing ratio of 0.6 ppm at depth, beginning a rapid decrease at about 1 bar. The PH_3 is believed to have been transported rapidly up from considerable depths, with the fall-off due to photolysis. A coupled treatment of PH_3 and NH_3 gives a reasonable match to the data. The phosphorus thus released may contribute to the coloration of the clouds. It is possible, therefore, that PH_3 and coloration may be anticorrelated, as they are measured by NIMS at 5 μm and in images and photometry by SSI and PPR. On the Probe, the NMS should be able to measure PH_3 by use of its Sample Enrichment System and improve on the absolute accuracy of the existing remote measurements.

The abundance of sulfur on Jupiter and the vertical profile of sulfur compounds are also fundamental for understanding the evolution and present state of the atmosphere. H_2S is expected to be the predominant sulfur compound at depth (Lewis, 1969b), but it has not been observed on Jupiter to date possibly because it is converted to other sulfur compounds such as NH_4HS and precipitated from the upper levels of the atmosphere. Weidenschilling and Lewis (1973) predicted the existence of such clouds at about the 1.8 bar level (Figure 1), but Sato and Hansen (1979) have shown that this part of the atmosphere is sufficiently transparent to permit penetration of a substantial amount of sunlight to depths of at least 3 bars. However, Bezard *et al.* (1983) conclude that cold 5-μm spectra require a moderately thick cloud layer located in the 1- to 4-bar range, and that the most likely candidate for this cloud constituent is NH_4SH. The Probe NMS should determine the abundance of H_2S with a precision of a factor of 2 or better.

Information on other gaseous constituents should be obtained by the NMS. It is planned to measure peak intensities of all mass numbers in the range 1–150 AMU, although spending most of the time in the 1–52 range. The nominal dynamic range of 10^8 will permit measurement of peaks in the amount of 10 to 100 parts per billion, but the instrument background and overlapping mass spectra may raise the detection threshold depending on the environment actually encountered in flight.

The IRIS experiment on Voyagers 1 and 2 detected both temporal and spatial variations of stratospheric hydrocarbon composition based on data between 4 and 55 μm. In particular it found that the ethane/acetylene ratio (C_2H_6/C_2H_2) increased by 70% in the four months between the two flybys, and that the same ratio was about three times larger at 60–70° latitude than at low latitudes (Hanel *et al.*, 1979b). The Galileo Orbiter will have the capability to monitor composition changes over an extended time period and to observe spatial variations over the planet, which will provide important constraints on chemical and transport processes. These results may however not extend to stratospheric heights.

Occultation measurements from the Galileo orbiter, including occultation of the Sun, the Earth, the Galilean satellites and bright stars provide opportunities to obtain compositional information at relatively high altitudes in the Jovian atmosphere. Radio Science (RS), UVS, NIMS, PPR, and SSI all are capable of employing this technique, which is based on measurement of absorption of radiation occurring on the long slant path through the atmosphere at the time of occultation. It should be possible to obtain an indication of latitudinal variations of composition by observing several occultations. Longitudinal variations, which are not unlikely for the stratospheric and mesospheric regions accessible by occultation, can be investigated from the immersion and emersion results.

2.2. Thermal structure

Mean temperature profile. The first-order question regarding atmospheric temperatures is the mean vertical profile. Along with the major composition, which is nearly constant, it determines the structure of the atmosphere, and indeed of the entire planet. Jupiter's large internal heat flux ensures that the lapse rate at depth is essentially the adiabatic value; the entire scale will be determined by the measurements made in the 1–10 bar region. Nevertheless, small deviations from the adiabat are extremely important as indicators of the controlling processes, such as local vertical convection or circulations on a much larger, perhaps even global, scale. The convective-radiative boundary probably lies near 700 mb; at greater altitudes planetary thermal radiation and solar heating bring the gradient to zero (the tropopause) and then turn it positive.

Information from Voyager is summarized in Figure 1 which, however, omits the marked and variable structure seen in radio occultation (Lindal *et al.*, 1981) in the lower stratosphere. The Atmospheric Structure Instrument (ASI) on the Galileo Probe will measure the temperature-pressure profile using acceleration, temperature and pressure sensors. Data will be obtained from about 750 km above the cloud tops to about the 1 bar level with continuous definition, greater accuracy, and much higher vertical resolution than previous measurements, and the vertical profile will continue downward to at least the 10 bar level. The Probe will obtain its data at a single location within 5° of the equator. The Orbiter measurements, which will overlap the Probe measurements down to almost the 1 bar level, can characterize the site of Probe entry in relation to other locations. Orbiter measurements of the temperature structure throughout the Galileo mission will define a more meaningful time mean structure for low latitudes and for the whole globe if inclined orbits are obtained during an extended mission.

Temperature measurements and inferences from Orbiter instruments are important for placing the Probe results in a global context, but also have several important roles of their own to play. The atmospheric temperature, along with the winds and clouds (with possible accompanying precipitation), define the basic weather and climate of Jupiter. The temperature profile and the variation of temperature along constant pressure surfaces are crucial for analyzing the atmospheric general circulation. Temperature measurement, together with the radiation budget, cloud properties and winds inferred from high-resolution imaging, are also important for analyzing processes

occurring in local features such as the Great Red Spot, white ovals, and hot spots, including the brown 'barges'. Temperatures can be obtained over longer time-scales than observed by either Pioneer or Voyager, and profiles can be contemporary with detailed studies of cloud properties and the radiation budget.

Orbiter measurements of temperature will be obtained from three instruments. The PPR experiment will use measurements through several filters in the 15–100 μm spectral region to obtain temperature profiles for pressure levels between about 60 and 600 mb at all locations observable from the orbiter. The NIMS experiment will retrieve temperatures from its measurements in the 5 μm spectral region. At low latitudes, up to at least $\pm 30°$, there are known to be large 5 μm 'hot spots', due to local transparency of the upper clouds, which should permit determination of temperatures in the 1–5 bar region (Terrile and Westphal, 1977). Finally, occasional occultations of the Earth by Jupiter will permit the RS experiment to determine temperature profiles for pressure levels between about 25 and 500 mb, at two locations per occultation event.

Horizontal temperature variations. The Infrared Radiometers on Pioneers 10 and 11 obtained several maps in the spin-scan mode through broad channels centered on 20 and 45 μm. In the latitude range 45 N–45 S, they revealed significant temperature differences between belts and zones and otherwise suggested a relatively small dependence on latitude within the range sampled (Orton and Ingersoll, 1976).

Horizontal variations of temperature on constant pressure surfaces have been obtained by the IRIS experiment on Voyager for low- and mid-latitudes between pressure levels of about 500 and 5 mb at two times. The results are valuable for interpreting the atmospheric dynamics on both the global and local scales (Pirraglia *et al.*, 1981; Flasar *et al.*, 1981).

Temperatures measured by Voyager in the upper troposphere and lower stratosphere showed substantial interhemispheric differences, wave-like vertical structure and differences between the two periods of observation (Hanel *et al.*, 1979a, b). According to one suggestion (Clark *et al.*, 1979) the interhemispheric differences and wave-like structure may be due to vertical wave propagation originating from the respective tropopause regions. A second suggestion (Caldwell *et al.*, 1979) is that the north–south temperature asymmetries and vertical structure arise from differences in local solar heating due to differences in aerosol opacities. Further analysis of aerosol heating (Appleby and Hogan, 1984) suggests that this may account for the stratospheric thermal structure shown by radio occultation measurements from Voyager. The measurements of temperature variations from the Galileo Orbiter, together with the measurements of aerosol properties, aerosol vertical profiles and the radiation budget, will make it possible to analyze these phenomena.

It will also be important to obtain the horizontal temperature patterns from the Galileo Orbiter and the 'ground truth' from the Probe for use in conjunction with other data obtained at that time. For example, the Galileo mission will obtain substantially improved information on cloud properties, vertical cloud layering, vertical wind shear and radiation budget. In order to take full advantage of these data for interpreting atmospheric processes it is necessary to have temperature profiles obtained at the same

time as the other Galileo observations. Because of the limited locations at which occultation and 5 μm temperatures will be obtained, the horizontal temperature distributions will be primarily those obtained by the PPR, which will be limited to approximately the 60–600 mb region.

Finally, the great importance of extending the measurement of horizontal temperature variations to higher latitudes cannot be overemphasized. The observed cloud patterns and their motions clearly suggest a change in the dynamical regime polewards of $\sim 45°$ latitude. Furthermore, to study the influence of the Coriolis force and its variations on the general circulation, for example, requires that the measurements extend to high latitudes where the force is strongest. Neither the Pioneer nor Voyager spacecraft obtained temperature fields poleward of middle latitudes, and it will not be possible to make such measurements from the Space Telescope.

Post-Voyager work at the Hawaii IRTF (Infrared Telescope Facility) has discovered a strong anomaly of thermal emission near the magnetic poles (Caldwell *et al.*, 1981). This effect was then also found in the Voyager IRIS spectra of the north polar region (Kim *et al.*, 1985); it seems to be due to enhanced temperatures in the upper stratosphere. The location immediately suggests the precipitation of energetic charged particles, although the required fluxes are formidable. Continued Earth-based studies are highly desirable.

2.3. Clouds, aerosols, lightning

Jupiter has a variety of cloud forms which provide excellent opportunities for studying cloud processes including interactions with atmospheric dynamics, radiation and chemistry. The discussion below includes the large-scale layered clouds, high-level haze layers, and local clouds associated with features such as the Great Red Spot, white plumes and brown barges. We also include a discussion of lightning on Jupiter.

Cloud layers. Discussion of vertical cloud layering invariably begins with the pioneering work of Lewis (1969a). The assumption of thermochemical equilibrium in an atmosphere of solar composition leads to NH_3 clouds with their bottom at the level where $T \sim 145$ K, NH_4SH clouds at $T \sim 200$ K and H_2O clouds at $T \sim 270$ K. In Figure 1, the layers are shown relative to the Voyager IRIS temperature profile.

None of these clouds have been definitely identified on Jupiter. However, there is very strong circumstantial evidence that at least the white clouds in the zones (relatively bright latitudinal bands) are ammonia ice. Analysis of visible and near infrared spectral absorption bands by Sato and Hansen (1979) showed clouds at the appropriate level (~ 500–700 mb) and an amount of NH_3 gas beneath the clouds of solar or slightly greater abundance. Above the clouds, NH_3 is substantially depleted consistent with condensation at the lower temperatures and photolysis in the upper atmosphere. It is generally assumed that the zones are regions of rising motions which favor condensation while the belts (relatively dark latitudinal bands) are regions of sinking motions. Thus Terrile and Westphal (1977) conclude that ammonia clouds exist only in the zones, while in the belts one sees to a second layer which is presumably Lewis' NH_4SH cloud layer. This interpretation has the attractive feature of providing a possible explanation for the

color of the belts (Prinn and Owen, 1976), since solar illumination on solid NH_4SH may be able to produce yellow and brown colors (Lebofsky, 1974).

However, analyses of visible and near-infrared spectra indicate the presence of clouds in the 500–700 mb range over both the belts and zones, with the clouds over the belts having a smaller optical thickness and a smaller albedo for single scattering (Sato and Hansen, 1979). West and Tomasko (1980) have produced a detailed cloud model for different regions on Jupiter based on near-infrared images within several methane bands and continuum positions. Their results (Figure 2) also show clouds in both the belts and zones at levels where ammonia condensation is expected.

Both sets of results must be reconsidered in view of the remeasurement of the strengths of the H_2 quadrupole lines 3–0 S(1) and 4–0 S(1) by Bragg *et al.* (1982). The new values differ by respective factors of 0.86 and 1.58 from those assumed in the

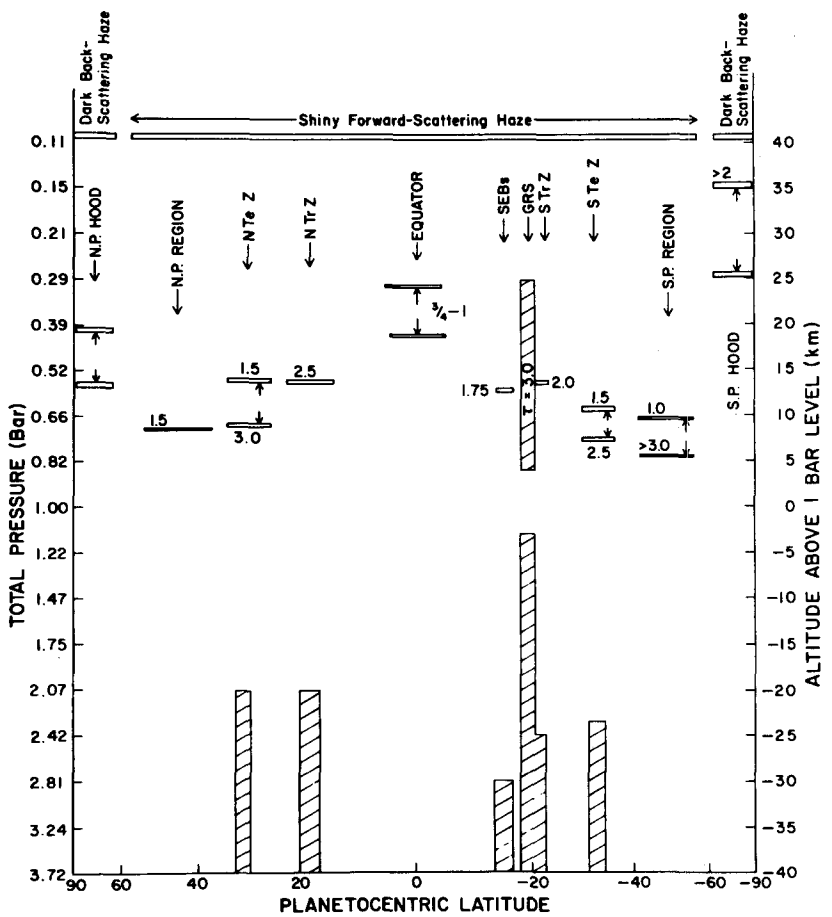

Fig. 2. Schematic representation of a computed global variation of cloud structure on Jupiter; the numbers for the upper cloud layer are estimates of cloud optical depth (after West and Tomasko, 1980). The models for the various latitudes were computed relative to an assumed model for the South Tropical Zone which was found to be consistent with methane absorption data and Pioneer Jupiter photometry.

analyses of Jupiter. West (private communication) has stated that his H_2 abundances, which scale all his other results, depend primarily on the 4–0 line, and should therefore be reduced by the factor of 1/1.58. His CH_4 mixing ratio (West, 1979) becomes 1.9×10^{-3}, and the upper cloud is located at 350 mb, with a clear space extending down to 1.4 bars. Smith and Tomasko (1984) find a similar height for the upper cloud, based on Pioneer polarimetry. The Sato and Hansen model cannot be adjusted so simply, because it was fitted to both H_2 lines. More recent analysis, based on imaging and IRIS observations from Voyager 1, has been carried out by West *et al.* (1985).

Sato and Hansen (1979) found that the region beneath the ammonia clouds must be relatively transparent to a depth of 3–5 bars in order for the amount of absorption in weak methane and hydrogen lines to be as great as observed. This constraint does not exclude NH_4SH clouds, expected to occur near the 1.8 bar level (Figure 1), but it implies that they are not optically thick as assumed in early multilayer cloud models for Jupiter. The requirement of a reflecting level at 3–5 bars is consistent with the expected location of H_2O clouds. However, from an analysis of cold 5-μm spectra, Bezard *et al.* (1983) find that a moderately thick cloud layer should exist within the 1- to 4-bar range and

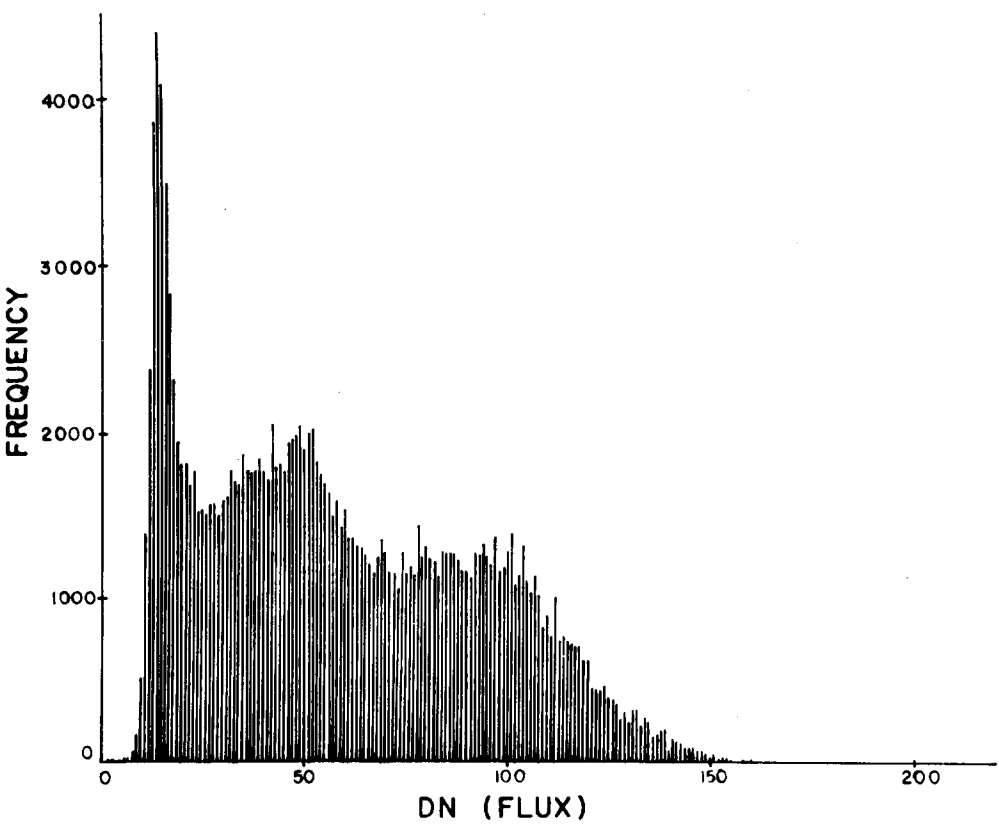

Fig. 3. Flux-frequency histogram of the central portion ($\mu > 0.95$) of Jupiter at 5 μm (Terrile and Westphal, 1977).

that NH_4SH is the most likely cloud constituent for this layer. Any such layer must be consistent with Voyager's ability to obtain images of lightning flashes. As mentioned above, West's reconsideration of West and Tomasko (1980) finds that the clear space extends only down to 1.4 bars. He feels that there is probably a range of fits to the data, with the end members having a thin upper cloud (optical depth 2) and a lower cloud top at 1.4 bars, and a thick upper cloud with a deep lower cloud top.

Valuable information on the vertical distribution of cloud layers beneath the ammonia cloud region comes from observations in the 5-μm spectral range (Gillett *et al.*, 1969; Keay *et al.*, 1973; Westphal *et al.*, 1974; Terrile and Westphal, 1977; Terrile *et al.*, 1978, 1979; Kunde *et al.*, 1982). These data show local regions of high 5 μm emission, suggesting the presence of holes in the upper clouds through which radiation from hotter levels below can emerge. The zones and Great Red Spot are cold regions, the belts are warmer, and local features in the equatorial region, identified in visible images with the blue-grey areas in the North Equatorial Belt, are the hottest.

Figure 3 shows Terrile and Westphal's (1977) histogram of 5 μm brightness temperatures for an area near the center of the disk including the Equatorial Region and the North and South Equatorial Belts. The histogram is trimodal with one strong peak and two weaker ones, which suggests the possibility of emission from different cloud levels in the atmosphere. The highest brightness temperature obtained (data number ~ 150) was reported by Terrile and Westpahl to be ~ 260 K. The corresponding temperatures of the three peaks are ~ 250, 225 and 200 K. However, the observed 5-μm limb darkening suggests that it is necessary to account for absorption and re-emission above the radiating levels. Terrile (1978) did this and obtained the temperatures of the three radiating levels as 292, 225, and ~ 140 K. These results depend upon assumptions about the presence or absence of different cloud layers. More recent work has shown that the ammonia cloud is almost transparent at 5 μm and there is no problem in detecting 'hot spots' through it (West and Tomasko, 1980; Orton *et al.*, 1982; Bezard *et al.*, 1983; Smith and Tomasko, 1984).

The Galileo Probe is well instrumented to measure the properties of the clouds it passes through. The primary instrument is the Nephelometer (NEP) which will measure bulk scattering at five angles. The results include not only optical depth as a function of pressure, but also the size distribution and optical properties of the particles. A different view of location and attenuation is provided by the Net Flux Radiometer (NFR). As mentioned in the previous section, compositional information will be obtained by measuring the vapors with the NMS, and from the location of the clouds on the temperature profile determined by the ASI.

It is in the area of cloud science that the synergism of Probe and Orbiter experiments is strongest. As both vehicles approach the planet, the entry site will be studied each time it rotates under the Orbiter. At this time, as well as later in the mission, accurate measurements of emitting temperatures in the 5-μm region by NIMS will be a valuable aid for understanding the cloud structure, particularly when obtained with SSI high resolution images and PPR polarization measurements of the cloudtop pressure for the upper cloud. NIMS, PPR, and SSI multiband photometry will provide additional

constraints on the vertical cloud structure beneath the upper cloud layer. Taken together, these measurements should provide a good indication of cloud layering down to depths of a few bars. The probe observations can provide 'ground-truth' required to verify inversion procedures for Orbiter data, making it possible to extend Probe observations to other regions with confidence.

All of the major cloud layers predicted for Jupiter (NH_3, NH_4SH, H_2O) are normally white, i.e., nonabsorbing in the visible spectrum. Thus a key question about the clouds of Jupiter is the source of cloud coloration. A prime candidate is sulfur (e.g., S_8) or sulfur compounds [e.g., $(NH_4)_xS_y$ or H_xS_y] as suggested by Lewis and Prinn (1970, 1971). Red phosphorus (P_4), suggested by Prinn and Lewis (1975) as the cause of the Red Spot's color (see below), and phosphorus compounds could also be involved. Other suggestions including organic substances are discussed by Sill (1976) and Prinn and Owen (1976).

Identification of the composition of the upper cloud layer in the region of Probe entry is highly probable, with mass spectrometer data (NMS), cloud temperatures (ASI), and cloud particle sizes and number densities (NEP) from the Probe, together with information on the cloud particle size, shape and refractive index from photopolarimetry (PPR), large-scale cloud morphology from high-resolution imaging (SSI), and infrared (NIMS), and ultraviolet (UVS) spectral properties from the Orbiter. The Probe and Orbiter will provide complementary information and valuable cross-checks. Such information will be critical for evaluation of temperature and compositional profiles for the upper troposphere from the PPR and NIMS experiments (Orton *et al.*, 1982). Extension of cloud identification to other regions on the planet by the Orbiter and to substantial depths by the Probe will depend upon the nature of the circumstances encountered, but chances of success will be improved by a good overlap of Probe and Orbiter data.

High haze layers. A large number of different observations have indicated the existence of haze layers in the Jupiter atmosphere above the main visible cloud deck. Haze exists over a large range of altitudes in the upper troposphere and throughout the stratosphere. There is also evidence that the haze properties differ from one location on the planet to another and that they change with time.

The existence of *stratospheric* haze is indicated by slant path observations during lunar eclipses (Smith *et al.*, 1977) and stellar occultations (Cook *et al.*, 1979a, b). It is also evident by its strong effect in reducing the albedo of the planet in the blue and ultraviolet (Axel, 1972). The optical thickness of haze above the tropopause ($P \sim 100$ mb) is apparently small, of the order of a few hundredths. It is nevertheless significant for local radiative heating, and there may be substantial variations in its opacity with latitude and time (Caldwell *et al.*, 1979; West *et al.*, 1981). Images within and outside of a methane band (Owen, 1969; West, 1979) indicate the presence of a polar-cap haze, which varies with time. A pole-to-pole photometric scan at ~ 240 nm from Voyager 2 also suggested the presence of stratospheric absorption, either molecular or particulate (Hord *et al.*, 1979; West *et al.*, 1981). Analysis of Pioneer polarization data by Smith and Tomasko (1984) confirms most of these results, suggesting an optical depth of a few tenths at an

effective level around 100 mb. Information on the haze particle physical properties, the vertical and horizontal haze distribution and the nature of its temporal variations may help identify the source of the haze and determine its role in stratospheric heating and dynamics. The heating has most recently been studied by Appleby and Hogan (1984), who confirm that it must be included to obtain a good match with the structure seen in Voyager radio occultations.

There is a substantial *tropospheric* haze above the main ammonia cloud region (500–700 mb). Figure 4 shows cloudtop altitudes deducted by Coffeen (1974) for

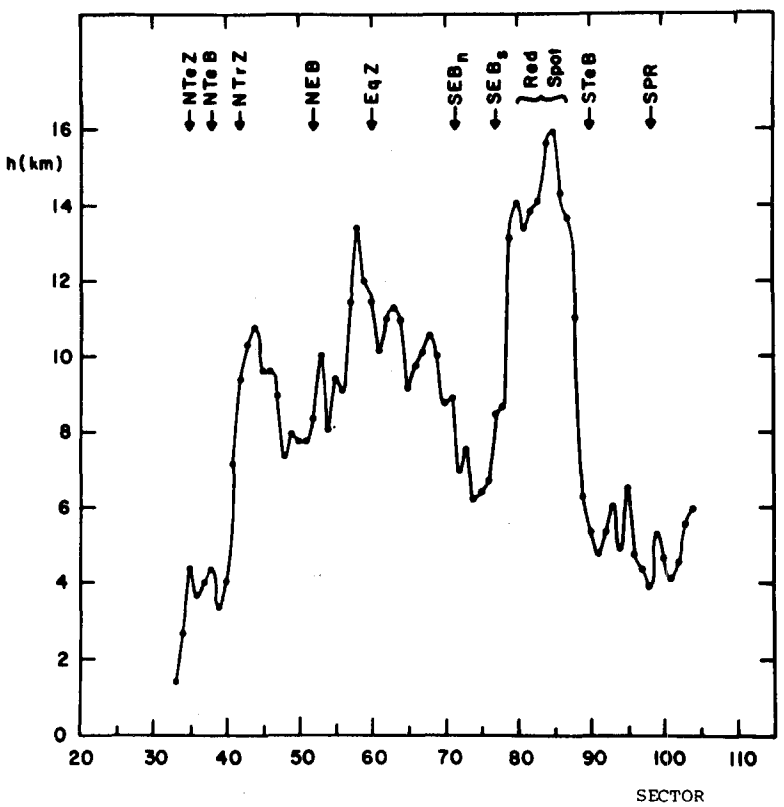

Fig. 4. Jupiter cloudtop altitudes (above the 650 mb level) based on the assumption of Rayleigh scattering above a Lambert surface. (Coffeen, 1974).

different regions on Jupiter from a Pioneer 10 North-South polarization scan; these altitudes were obtained on the assumption of pure Rayleigh scattering above a Lambertian reflector. They should thus be interpreted as an approximate indication of the level at which an aerosol optical depth of unity is reached, which is influenced both by real cloud height variations and the amount of diffuse haze in the upper troposphere. One plausible interpretation of the slightly higher altitudes for the zones in Figure 4 is that these regions contain ammonia cirrus layers; this would be consistent with the relative whiteness of the zones. So far there is little quantitative data available with

which to judge the physical properties of the haze particles on Jupiter. Perhaps the most promising source is Pioneer 10 and 11 polarimetry, which indicates, for example, that the aerosols in the upper troposphere in the SEB are about 0.2 μm in radius (Stoll and Tomasko, 1979).

The Galileo mission will obtain information on the tropospheric haze from both the Probe and Orbiter and on the stratospheric haze from the Orbiter. The Probe Nephelometer measurements of aerosol size and optical thickness will begin at about the 100 mb level. The Net Flux Radiometer will provide information on the aerosol absorption properties and the Neutral Mass Spectrometer will yield information related to the aerosol chemical composition. For the same reasons as discussed for the cloud layers, it will be important to have simultaneous Orbiter measurements of the probe entry site. Cross-calibration with the Probe and extension of aerosol data to the global scale can be performed well by the Orbiter because the region $\sim 100-500$ mb can be probed readily with the same optical measurements discussed above for the clouds. Satellite and stellar occultation measurements can also be made to determine aerosol layering in the stratosphere.

Local cloud features. Features such as the Great Red Spot, white ovals, brown barges, and white plumes are of special interest because they may be able to tell us a good deal about the atmospheric dynamics, cloud physics, and composition, possibly including information on levels of the atmosphere which would otherwise be difficult to observe. The Red Spot, for example, may involve convection which brings up materials from depth which are far out of local thermochemical equilibrium. The equatorial plumes may be a special type of convective activity (Hunt *et al.*, 1981).

Such local features can only be investigated by the Orbiter. The primary measurements will be those discussed above for the SSI, PPR, NIMS, and UVS instruments. In addition to the several different measurements providing information on the cloud and haze properties, the determination of temperature profiles and horizontal variations of temperature by PPR and NIMS will be particularly useful for studies of processes. Rapid sequences of high-resolution images by SSI will permit determination of atmospheric winds and their shear, while the PPR will measure the radiation from the features in comparison with surrounding areas.

Lightning. Most lighting on Earth is produced by the charge generated and separated by cumulonimbus clouds, which are ice-water convective clouds initiated by vertical moist static instability. As the moist air rises and cools, condensation, and ultimately precipitation, occur. The collisions between water and ice leave some particles charged positively, some negatively. It is thought that the positive charges are predominantly on the smaller particles which are preferentially raised aloft by vertical convective motion, with heavier, negatively charged particles precipitating. Most lightning discharges in the Earth's atmosphere occur within a cloud cell (intracloud lightning) and neutralize tens of coulombs of charge (e.g., Uman, 1969).

The cloud model of Lewis (cf. Figure 1), with water ice and liquid water layers, suggests that a similar dynamic regime can exist within the Jovian cloud system (e.g., reviews by Rinnert, 1983; Williams *et al.*, 1983). The detection of lightning on Jupiter

by the Voyager spacecraft (Smith *et al.*, 1979a; Cook *et al.*, 1979b, Gurnett *et al.*, 1979) supports this hypothesis. The fact that an atmospheric level is capable of producing the violent conditions believed to be a necessary pre-requisite for lightning has implications for the vertical static stability and large-scale atmospheric dynamics at these levels. Observations from Galileo can determine the frequency and global distribution of lightning on Jupiter and the typical sizes of the storms. If such storms on Jupiter are analogous to those on Earth, this type of information could indicate the conditional stability or instability of the cloud regions, regions of large-scale convergence and divergence, and the time- and length-scales associated with the cloud dynamics in the region where the lightning originates. It will be particularly interesting to compare different atmospheric regions (belts, zones, spots) and to study the time variations of lightning statistics in each region and their relationships to observed changes in atmosphere dynamics, cloud properties, and radiation budget.

The primary experiments on Galileo for measuring lightning are the Lightning and Radio Emission Detector (LRD) on the Probe and the imaging system (SSI) on the Orbiter, which are complementary. The LRD measurements will be able to verify the existence of lightning and measure its intensity, flashing rate, and radio emission, at a range up to about 10^4 km (Rinnert *et al.*, 1981, 1984; Lanzerotti *et al.*, 1983). The LRD data will be obtained during the entire Probe descent, including inside and below dense cloud systems where Orbiter imaging will not be possible. Cloud images from the Orbiter will relate the probe entry region conditions to the global situation. Images of lightning from the dark side of the planet in combination with the measurements by the LRD will allow inference of the global lightning distribution.

2.4. Radiation Budget

Radiation budget information is fundamental to understanding Jupiter's internal structure, atmospheric dynamics and vertical atmospheric structure. The following discussion is organized into sections on the global radiation budget (i.e., magnitude of internal energy source), meridional and local radiation balance and vertical profile of radiative heating and cooling.

Internal energy source. The magnitude of Jupiter's internal heat source constrains models of the internal structure of Jupiter (Cameron and Pollack, 1976) and its evolution. Furthermore, Stone (1972) and Gierasch (1976) have shown that the atmospheric dynamical regime is crucially dependent on the magnitude of the internal heat source.

Recent estimates of the ratio of emitted flux to absorbed flux range from 1.67 to 2.5 (Tomasko *et al.*, 1974, 1978; Ingersoll *et al.*, 1976). The Voyager value 1.67 (Hanel *et al.*, 1981) is the lowest. However, the actual value may lie outside that range, since true radiation budget measurements of Jupiter have not been made. Determination of the radiation budget requires knowledge of the outgoing reflected solar and emitted thermal radiation in all directions integrated over all wavelengths. Measurements to date have been near the equatorial plane except for Pioneer 11. The two Pioneers had only two narrow-band solar channels (at about 0.45 and 0.65 μm) and two broader thermal

channels (at about 20 and 45 μm), and since the thermal instrument was not pointable, maps of the planet were obtained from only two directions. Voyager carried a radiometer covering the 0.4–2 μm range and a far-infrared interferometer covering 4–50 μm; however, the data were all obtained from near the equatorial plane.

The Pioneer thermal measurements showed little variation with latitude, leading Ingersoll and Porco (1978) to suggest that internal heat flow may be distributed with latitude so as to make the sum of absorbed solar energy and internal heat flow independent of latitude. This would require the total planetary thermal emission to be at least $4/\pi$ (~ 1.3) times the total solar absorption, for latitude-independent Bond albedo. However, with the angular and spectral limitations of the Pioneer radiation budget data, the speculations derived from it are very tentative.

While the Galileo instruments offer more complete spectral coverage than Voyager, its primary mission in the equatorial plane cannot improve the latitude coverage. In principle an extended mission may offer the ability to transfer to a higher inclination.

Meridional and local radiation budget. The latitudinal variation of the radiation budget is a fundamental diagnostic for the meridional transports of energy by a planet. On the Earth, high accuracy ($\sim 5\%$) radiation budget data provide the best information we have on ocean heat transport (Oort and Vonder Haar, 1976); poleward transport is obtained as the difference between the radiation budget and the atmospheric transport, the latter calculated from observed temperatures and winds. A similar procedure has been used on Jupiter to obtain the latitudinal variation of the internal heat source at a level just below the region of solar energy deposition (Ingersoll and Porco, 1978).

Key questions related to the meridional and local radiation budget are: How do the solar heating and net radiative heating vary horizontally? Does the thermal emission vary with latitude? Do horizontal variations of solar radiation absorbed by stratospheric aerosols give rise to horizontal temperature gradients which contribute to stratospheric dynamics? Do belt-zone heating contrasts contribute a dynamical drive which feeds back on the belt-zone structure? What causes the belts and zones (cf. Section 2.5)? The local radiation budget will provide an important diagnostic for the latter problem, since it will suggest whether or not there is an energy exchange between the belts and zones. Similarly, in analyzing a regional phenomenon such as the Great Red Spot it will be important to know whether that region is a relative source or sink of energy. In addition, knowledge of the vertical profiles of radiative heating at different locations can be obtained (see below) if the atmospheric composition and cloud properties are known at each location.

All comments about the Galileo mission's ability to obtain global radiation budget measurements are also applicable to meridional and local radiation budget measurements.

Vertical profile of radiative heating. Absorbed solar radiation and the flux of energy from the planet's interior are the main sources of energy for the dynamics of Jupiter's atmosphere. Knowledge of the vertical profile of solar energy deposition in the atmosphere, the vertical profile of net radiative heating/cooling, and horizontal variations of these profiles are needed for analyzing both local convective processes, including lightning, and the large scale dynamics.

One question is the level below which radiative transfer is unable to carry the vertical energy flux being transported by the atmosphere. If the vertical profile of solar energy deposition and the atmospheric composition are known, the answer to this question can be readily computed with a one-dimensional radiative-convective model. The greatest uncertainty in current estimates for the vertical profile of solar energy deposition is due to our ignorance of the levels at which the continuum absorption occurs. Additional uncertainty stems from the lack of detailed knowledge of the vertical distribution of clouds and aerosols.

Observations of the vertical profiles of solar heating and net radiative heating will be obtained by the Net Flux Radiometer (NFR) on the Probe. Since the Probe will begin measurements at about the 100 mb level, measurements of the same region from the Orbiter are required for extension to the top of the atmosphere (Lacis and Hansen, 1974). To accomplish this the PPR radiation budget channels (total reflected solar and total emitted thermal) are the same as the NFR channels, and the primary PPR photopolarimetry band for analyzing cloud properties is located at 0.95 μm, close to the wavelength used by the NEP. The PPR measurements of radiative fluxes, vertical aerosol distribution, and aerosol sizes for the region above Probe operation will provide the radiative boundary conditions (angular and spectral distributions of the radiation) at the level where NFR measurements begin. With this support from the Orbiter, the Probe is expected to provide accurate radiative heating profiles and their correlation with cloud properties from the top of the atmosphere to a depth of several bars.

With the aid of the Probe results, the Orbiter observations can extend radiative heating determinations to other locations on the planet. For altitudes above approximately the 1 bar level, it should be possible to obtain reasonably accurate estimates of the radiative heating and cooling profiles from the Orbiter measurements of radiation budget, temperature profile, and cloud properties. However, in order for this procedure to be accurate and reliable, it is important for it to be tested and calibrated at the region of Probe entry. This reemphasizes the value of simultaneous Probe and Orbiter measurements. A gap in Galileo's wavelength coverage is the 7.8 μm band of methane, useful for sounding the stratosphere. A supplementary ground-based program will be valuable here.

2.5. Dynamics

Present observations of the atmospheric dynamics of Jupiter continue to pose a formidable challenge to theoretical understanding. The dominant global features of the atmospheric circulation include the strongly super-rotating equatorial current and at higher latitudes the axisymmetric and long-lived pattern of alternating westward and eastward jet streams. Smaller centers of motion include the Great Red Spot, the white ovals, and brown barges. The equatorial plumes and other periodic features at smaller scales suggest the presence of atmospheric wave activity. Turbulent convection is believed to be a pervasive feature of the atmospheric background at still smaller dimensions and is probably important for cloud electrification. A schematic summary of the range of space- and time-scales associated with various dynamical regimes is

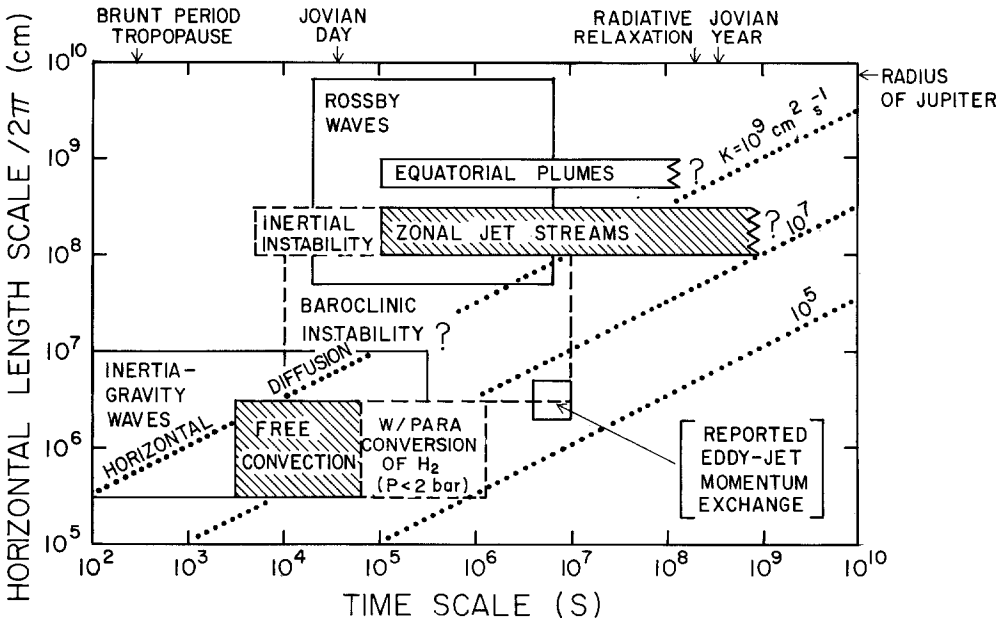

Fig. 5. Dynamical regimes on Jupiter (Allison and Gierasch, 1984).

indicated in Figure 5 (after Allison and Gierasch, 1984). Pre-Voyager assessments of Jupiter's dynamic meteorology are given by Stone (1976) and Ingersoll (1976).

The Voyager reconnaissance of Jupiter has added greatly to our knowledge of atmospheric motions at cloud level and the thermal fields aloft. Zonal velocities and a tentative assessment of eddy motion fields have been derived from cloud-tracked wind measurements between latitudes of $\pm$ 60 deg (Ingersoll *et al.*, 1981; Limaye *et al.*, 1982). The thermal wind analysis of Voyager IRIS data indicate a strong correlation between zonal motions and upper tropospheric temperatures in the sense required for a reduction of the strength of the jets with height (Pirraglia *et al.*, 1981). Recent analysis of the IRIS data indicates the disequilibrium of the *ortho-* and *para*-hydrogen states in Jupiter's upper troposphere and may suggest important modulations of the buoyancy contrasts at this level (Conrath and Gierasch, 1984).

The character of Jupiter's zonal flow at depth and its energetic drive remain inaccessible to observation, however. Two extreme theoretical pictures of the zonal flow are currently under investigation. In one view the axisymmetric pattern of alternating eastward and westward jet streams are the effect of counter-rotating cylinders of motion, concentric with the planetary spin-axis, and extending throughout the bulk of the interior molecular-hydrogen envelope (e.g., Ingersoll and Pollard, 1982; Busse, 1983). In the other view the zonal flow is confined to a thin shell in the vicinity of the cloud layers, with geostrophic winds balanced by thermal contrasts (e.g., Allison and Gierasch, 1982; Gierasch, 1983). Both pictures of the dynamics thus far lack a complete theory which can satisfactorily account for all the observations. Fundamental uncertainties include

the nature of zonal flow instabilities (e.g., Conrath *et al.*, 1981) and the nonlinear exchange between waves and mean flow suggested by numerical models (Williams, 1978, 1979).

Progress in resolving these problems will require a better knowledge of the three-dimensional wind and temperature fields, and some determination of the thermodynamic effects of cloud condensation and other phase changes such as the ortho- to para-conversion of hydrogen. Observations of atmospheric waves and other synoptic scale features will bear upon important parts of the problem and may offer an indirect means of diagnosing the stratification and eddy exchanges which determine the global dynamics (cf. Allison, 1983).

A prime atmospheric dynamics objective of the Galileo mission is to explore the vertical dimension by means of Probe measurements at a single point and Orbiter measurements employing the spectral capabilities of several remote sensing instruments. The Probe will obtain the temperature profile to a depth of at least 10 bars, as well as the composition, cloud structure and radiation balance measurements described in other sections of this paper. The Orbiter will measure the temperature profile, as well as cloud and radiative properties, at many different locations including the entry Probe region, but with less resolution and not to as great a depth as the Probe. It may also be possible to assess the *ortho-para* fraction of hydrogen at selected locations from the infrared sounding channels of PPR, or from the Earth. Valuable information on the vertical variation of horizontal wind speed at one location will be obtained by Doppler shift tracking of the Probe's descent, and at other locations by the vertical discrimination provided by the spectral pass-bands of SSI, the polarimetry and methane-band photometry of PPR, and the near-infrared measurements of NIMS. Measurements of the Probe entry region by the Orbiter will provide an important *in situ* verification of remote sensing capabilities. The continued reconnaissance of the atmosphere by the Orbiter instruments will then provide the spatial coverage and long time base essential for the diagnostic analysis of global dynamical regimes (cf. Figure 5).

The concerted analysis of the Galileo measurements will address several key questions concerning the atmospheric dynamics. How do stratospheric dynamics couple to the troposphere? What are the correlations between temperature, cloud variations, ortho-para fraction, and dynamics? To what extent are the heat and momentum balances controlled by wave dynamics? How are the large-scale vorticity-conserving motions coupled to small scale convection?

The Galileo reconnaissance of Jupiter's atmosphere can be usefully supported by Space Telescope imaging with sufficient spatial resolution to assist in target identification, navigational pointing assessment, and eddy-mean flow analysis on a global scale over a long time base. Ground-based imaging and infrared measurements in the 5 μm region will provide additional mission support.

2.6. Upper atmosphere, ionosphere, magnetosphere-atmosphere interaction

Current knowledge. The albedo of Jupiter at Lyman-alpha (1216 Å) has been measured several times, using the Copernicus and IUE satellites and the Pioneer 10 and Voyager flybys. Since the polyatomic molecule CH_4 absorbs strongly at 122 nm, solar Lyman-alpha is absorbed below the homopause. Above the homopause these heavy molecules rapidly disappear and the solar Lyman-alpha photons are scattered by the ambient atomic hydrogen. The abundance of this gas depends on the column rate of dissociation of H_2 (which is closely related to ionization and the subsequent recombination of H-bearing ions) and the strength of vertical mixing. Estimates of K, the vertical eddy mixing coefficient, derived from albedo measurements, range from 3×10^7 cm^2 s^{-1} (Pioneer 10) to 1×10^6 (Voyager). However, these estimates ignore the contribution of auroral processes to the dissociation of H_2. It is possible that the Pioneer Lyman-alpha brightness, obtained when the Jovian magnetosphere was apparently 'quiet', is closer to the true value than the larger values obtained when the auroral contribution overwhelmed the dissociation due to solar EUV.

Radio occultation measurements of the ionospheric electron density profiles have been performed by the Pioneer and Voyager flybys. The profiles are consistent with high exospheric temperatures of order 1000 K, far above the pre-Pioneer estimates of 100–200 K. The theoretical interpretation of the profiles is incomplete. Because the ion H_2^+ recombines very slowly, minor constituents that react with H_2^+ can profoundly affect the profiles, especially at lower altitudes; the overall profile also depends on the rate of ionization and depth of penetration of auroral particle streams. The Voyager occultation experiment also indicates that the ionization in the auroral zones is very inhomogeneous, as on Earth.

The highest-quality data on the upper atmosphere available to date came from the Voyager UVS experiments (Broadfoot *et al.*, 1981). These data have been used to detect and measure the spatial variation of the Lyman-alpha line of atomic hydrogen and the Lyman and Werner bands of H_2. In addition, some unidentified features exist in the vacuum UV spectra, notably at 157 nm. Helium is seen at 58 nm. Auroral zones near both poles have been observed in all the hydrogen emissions; the equatorward boundaries of these zones coincide with the locus of the feet of the magnetic field lines that intersect the Io torus. Precipitated fluxes of order 70 erg cm^{-2} s^{-1} (comparable to an IBC III aurora on Earth) are deduced from the emission intensities. The day airglow also contains all three emissions, but their intensities are far in excess of what could be produced by solar EUV alone; a widespread precipitated flux of ~ 5 erg cm^{-2} s^{-1} is indicated (compared to the solar EUV flux of less than 0.2 erg cm^{-2} s^{-1}). Mysteriously, the emissions from H_2 disappear on the night side (flux less than 1 erg cm^{-2} s^{-1}), although a weak Lyman-alpha emission remains. These charged-particle fluxes may be the dominant heat sources for the dayside and polar thermosphere.

In addition to these measurements of atmospheric emissions, the Voyager 1 UVS obtained a solar occultation, and Voyager 2 a stellar occultation (McConnell *et al.*,

1982). The principal result is that the ionospheric peak observed in the radio experiment is 1000 km higher than the level computed from the observed neutral densities. Rapid upward transport of ions and electrons is the suggested explanation.

Galileo will carry a UVS optimized for longer wavelengths, 120–430 nm instead of 55–150 nm. In most of the overlap region the sensitivity of Galileo is much higher. The Galileo spacecraft will undergo a limited number of occultations as seen from Earth, which will allow the first two-frequency measurements of the neutral atmosphere and ionosphere. In addition, other plasma wave phenomena, such as whistlers, can be monitored by Galileo to provide information on the ionosphere.

A sounding of the upper atmosphere will be made by the Probe Atmosphere Structure Instrument (ASI), which has an estimated density threshold at 10^{-14} g cm^{-3}. This threshold is expected to be crossed $\sim$750 km above the 1 bar level. Below this altitude, profiles of pressure, density, and temperature will be measured and derived from the data, continuously to the end of the Probe mission at 10 to 20 bars. The Probe traverse of the upper atmosphere is expected to define the state properties far more completely and accurately than they have been previously known.

The major tasks for Galileo will be to determine the state of Jupiter's upper atmosphere and its coupling to the magnetosphere in 1996 and to compare this with information from Voyager in 1979, Pioneer in 1974, and from Earth-orbit experiments. The specific parameters to be determined are: the location of the hompause; the importance of minor constituents in the lower ionosphere; the exospheric temperature; the morphology, particle energy, and energy fluxes of the auroral zones; the morphology and energy fluxes of 'non-auroral' precipitation; the degree and nature of day–night anisotropies; and the existence and interpretation of auroral and non-auroral emissions at wavelengths up to 430 nm. Of particular importance is the interpretation of the upper-atmospheric emissions in terms of magnetospheric interactions, especially the puzzle of the seeming confinement of precipitation to the day side.

2.7. Satellite Atmospheres

Io has enough atmosphere to support the ionospheres detected at both limbs by Pioneer 10 (Kliore *et al.*, 1975). Absorption by SO_2 was detected by the Voyager IRIS (Pearl *et al.*, 1979). There is, however, a large uncertainty in the pressure, since the Voyager observation (and perhaps also Pioneer) may have included gas in an erupting plume. The points of view are summarized by Kumar and Hunten (1982) and Fanale *et al.* (1982). Surface pressures on the day side are probably 10^{-5} to 10^{-3} microbar. There should also be O_2 of photochemical origin (Kumar, 1982), but the amount is very uncertain.

Io's plasma torus is discussed at length in the accompanying article on the magnetosphere (Frank *et al.*, 1987). Its composition, mainly ions of S and O, undoubtedly reflects the composition of Io's atmosphere. These ions radiate intensely in the far ultraviolet and were studied in detail by the Voyager UVS. No emissions from Io itself were detected, partly because of masking by the torus emissions, and partly because interference from the radiation belt prevented the instrument from being operated near Io. Neutral Na and K have also been detected from Earth.

The Galileo UVS, though operating at longer wavelengths, should still be able to observe the torus. Observations of Io's atmosphere will suffer the same problems as Voyager, but if successful should be very informative. In addition, a strong O_2 emission at 1.27 μm may be detectable by NIMS.

The other three Galilean satellites should all have small quantities of H_2O vapor and larger amounts of O_2 derived by photochemistry (Yung and McElroy, 1977; Kumar and Hunten, 1982). Some upper limits were set by the Voyager UVS (Broadfoot *et al.*, 1981), but considerably better sensitivity should be possible with the Galileo instrument. Again, the infrared O_2 band will be sought by NIMS.

3. Galileo Atmospheric Experiments and Studies

The purpose of this section is to describe the observations and studies which are planned from the Galileo Orbiter and Probe in sufficient detail to indicate their capability for satisfying the Galileo atmospheric science objectives.

3.1. Probe investigations

All six scientific instruments on the Probe have as their objectives study of the Jupiter atmosphere beginning at about 100 mb and extending to at least 10 bars depth. There is a high probability of successful operation to about 16 bars, reached some 48 min after passing the 0.1 bar level. Operation may be extendable to 60 min, i.e., to about 19 bars, depending on Orbiter requirements and the actual performance of the relay link from Probe to Orbiter. The parameters of the Probe science instruments are summarized in Table II.

TABLE II

Probe science instruments

Instrument	Mass (kg)	Power (W)	Volume (L)	Bit rate (b/s)
Atmosphere structure (ASI)	4.0	6.3	3.1	18
Nephelometer (NEP)	4.8	13.5	4.6	10
Helium abundance (HAD)	1.4	1.1	2.3	4
Net flux radiometer (NRF)	3.0	10.0	4.6	16
Neutral mass spectrometer (NMS)	12.3	29.3	8.6	32
Lightning and RF emissions/ Energetic particles (LRD/EPI)	2.5	2.3	2.9	8
Totals	28.0	62.5	26.1	88

Three different atmospheric regimes are experienced by the Probe and its scientific instruments: pre-entry, entry and descent. Figure 6 defines these regimes superposed on a model atmospheric temperature-pressure profile. The Probe system turns on automatically during the pre-entry phase at about 8 R_J, or about 6 hr before entry, defined to be 450 km altitude (about 5×10^{-8} bar). During the *pre-entry* phase:

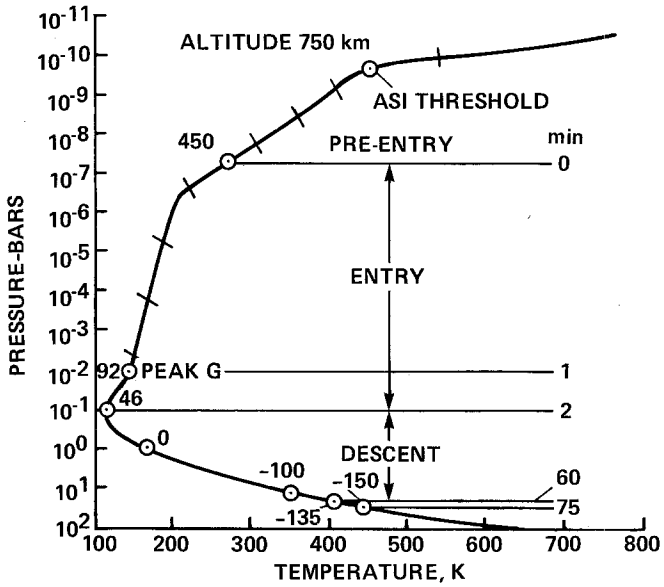

Fig. 6. Galileo Probe entry profile. 'ASI' is the Atmospheric Structure Instrument.

- The LRD makes observations at 4, 3, 2, 1 R_J.
- The EPI subsystem of LRD makes observations in the altitude range 4 R_J to 0.1 R_J.
- The ASI makes acceleration observations at altitudes below about 750 K (3×10^{-10} bar).
- The ASI and NEP make calibration runs.
- All data from the above are stored for relay to the Orbiter, thence to Earth during the descent phase.

During the 2 min *entry* phase from 5×10^{-8} bar to 0.1 bar, the only observations are of acceleration by the ASI, the data again being stored. During the *descent* phase all experiments, except EPI, are operational. The descent data are relayed to the Orbiter in real time, interleaved with the stored data from the pre-entry and entry regimes.

3.1.1. *Atmospheric Structure Instrument (ASI)*

PI: A. Seiff, D. B. Kirk, R. E. Young, S. C. Sommer, J. Mihalov (all at Ames Research Center), G. Schubert (Univ. of California at Los Angeles), R. C. Blanchard (Langley Research Center). Objectives: determine vertical profiles of state properties (temperature, pressure, density) from about 750 km altitude down to at least 10 bars. Ancillary objectives include: define temperature-pressure levels at which clouds form and provide diagnostics of phase change or chemical processes; test radiative balance measurements and models; define regions of adiabatic (convective) and sub-adiabatic (stable) lapse rates; define vertical flow velocities in regions of vigorous convective motion; detect turbulent fluctuations in temperature and atmospheric velocity; determine atmospheric

wave structures; determine mean molecular weight in regions of stable lapse rate and deep atmosphere.

Instrument: acceleration, temperature, and pressure sensors and associated electronics. Three-axis accelerometer (2 axial sensors, 2 lateral axis sensors), mounted near the center of gravity within the Probe, has four ranges: 0.0125, 0.4, 6.4, 410 g_E full scale. The temperature sensor is a dual platinum resistance thermometer mounted outside the Probe during descent in a region of high relative flow velocity. The sensor has a high heat-transfer coefficient and low thermal inertia so that it is well coupled to the atmosphere. The three pressure sensors sample pitot or total pressure outside the probe boundary layer during descent. Pressure is sensed from deflection of a thin stainless steel diaphragm which changes reluctance in a magnetic circuit. The pressure ranges of the three sensors are 0.5, 4, and 28 bars. The ASI parameters are summarized in Table III.

TABLE III

Atmosphere structure instrument
(ASI)
Parameter summary

– Typical altitude resolution	0.1 km
– Altitude difference accuracy	~1%
– Pressure accuracy	~1% of measured pressure
– Pressure dynamic range	0.1 to 28 bars
– Pressure resolution	0.1% of full scale on each range
– Temperature range	0 to 500 K
– Temperature accuracy	~1 K
– Temperature resolution	0.12 K (12 bit A/D conversion)
– Response times	T_1 16 ms – 5 ms, T_2 0.3 ms – 0.88 ms (Deployment to 16 bars)
– Vertical flow velocities, threshold	~1 m s^{-1}
– Acceleration dynamic range	3×10^{-6} to 4×10^{2} g_E
– Acceleration accuracy	within ~100 ppm

3.1.2. *Neutral Mass Spectrometer (NMS)*

P.I.: H.B. Niemann, R. E. Hartle, N. W. Spencer (all at Goddard Space Flight Center), S. K. Atreya, T. M. Donahue, G. R. Carignan (all at University of Michigan), D. M. Hunten (University of Arizona), and T. C. Owen (State University of New York). Objectives: determine abundances and isotope ratios of major (i.e., mixing ratio to hydrogen greater than about 10^{-7}) atmospheric constituents, as a function of altitude. Participate in cloud physics studies by providing abundance profiles for NH_3, H_2O, H_2S to aid in identification, location, and state of postulated clouds. Determine abundances and isotope ratios of trace (i.e., mixing ratio greater than about 10^{-8}) and noble gases as a function of altitude; search for the occurrence of less abundant species. Table IV lists NMS target species with indication of potential measurement precision.

Instrument: the sensor is a hyperbolic rod quadrupole with 15 cm long rods, 0.5 cm field radius; a dual filament electron impact ion source with three available electron energies; and a continuous channel secondary electron multiplier.

TABLE IV

Neutral mass spectrometer[a]

- Major gases: Assumed homogenous in atmosphere ($N(s)/N(H_2) > 10^{-7}$ H_2, He, CH_4.
  Will generate altitude profiles for these species.
  Isotope ratios measurable: D/H, $^2He/^4He$, $^{13}C/^{12}C$.
- Noble gases: From noble gas cell measurements He, Ne, Ar, Kr, Xe[b].
  Isotope ratios measurable: $^{22}Ne/^{20}Ne$, $^{38}Ar/^{36}Ar$.
  Isotope ratios possibly measurable: $^{21}Ne/^{22}Ne$, $^{82}Kr/^{84}Kr$, $^{83}Kr/^{84}Kr$, $^{86}Kr/^{84}Kr$.
- Gases with concentrations $>10^{-7}$ at some volumes of the atmosphere traversed (clouds/aerosols). H_2O, NH_3, H_2S, PH_3, HCN, C_2H_2, C_2H_6.
  Isotope ratios desired: $^{18}O/^{16}O$, $^{15}N/^{14}N$, $^{34}S/^{36}S$.
  Full altitude profiles not expected because of sensitivity limits of NMS.
- Other possible species (produced by photochemical reaction, or concentrated in the enrichment cells).
  Higher hydrocarbons; SiH_4, GeH_4, AsH_3, HCl, HBr, HI, CO, N_2, CO_2, CH_3S, $(C_2H_5S)_2$, CH_3CN, HCN, N_2H_4, P_2H_4, etc.
  Laboratory calibration accuracy $\pm 5\%$ for mixing ratios of $>10^{-4}$, $\pm 20\%$ for mixing ratios $10^{-4} > 10^{-7}$. Enrichment cell has potential for detecting mixing ratios of $>10^{-9}$ with factor of 2 accuracy.

[a] The precision and accuracy for all measurements in flight becomes a function of the complexity of the spectrum as well as the sensitivity of the NMS (e.g., CH_4–NH_3–H_2O or SiH_4–PH_3–H_2S).

[b] Xe may be detectable in either the rare gas cell or in the enrichment cell effluents.

Parameter summary

– Ambient pressure range	0.1 bar to 20 bar nominal
– Ion source pressure range	10^{-4} to 10^{-13} mbar
– Mass range	1 to 150 AMU
– Scan format	Stepping, single or half-mass 0.5 s per mass step nominal 60 s scan period (2 to 52 AMU) periodic scans to 150 AMU
– Resolution/cross talk	10^{-6} for adjacent half-mass at 20 AMU
– Dynamic range	10^8

The complete sample inlet system, shown schematically in Figure 7, consists of two fully self-contained units which operate in a timed sequence as the Probe descends through the atmosphere. Both units contain a high-pressure flow system whose gas inlet side is placed near the apex of the Probe, and whose exit ports are placed at the minimum pressure point inside the Probe. The pressure difference (approximately 6 mb) between the stagnation point and the low-pressure point causes a flow past the pressure reducing leaks. The inlet and outlet ports are sealed by metal-ceramic devices and kept under vacuum prior to entry. They will be opened in a pre-programmed sequence after atmospheric entry by pyrotechnic actuators. The measurement sequence is illustrated

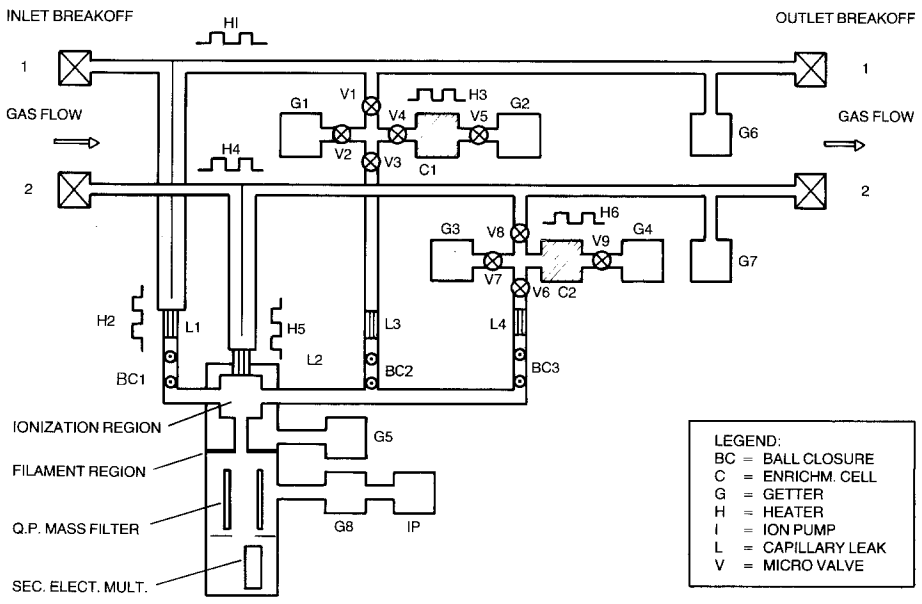

Fig. 7. Block diagram of the sample inlet system for the Neutral Mass Spectrometer.

in Figure 8 which shows the time-dependence of the total and ion-source pressures during Probe descent.

The direct gas inlet system is designed to minimize bias of the gas sampled. The measurement strategy involves obtaining spectra of the species and observing the variations in the fragmentation patterns obtained at different electron energies to increase the detection threshold or accuracy of the measurements.

A small fraction of the gas flowing through the high-pressure flow system is conducted through pressure-reducing leaks into the ionization region of the ion source. The leaks, which are arrays of micron-size glass capillaries (typically seven capillaries per leak), have conductances chosen so that the pressure in the ion source does not exceed 10^{-4} mb. A pure noble gas sample is prepared by utilization of chemical gettering action on a trapped atmospheric sample. The enrichment cells are packed with compounds which absorb trace gases such as H_2S, PH_3 and complex hydrocarbons. The gases absorbed by the cells are released by a programmed heating cycle during the Probe descent. During these cycles the cells are isolated from the flow system by microvalves and connected through separate capillary leaks to the ionization region. The second inlet system is opened to the atmosphere after the first system has been isolated from the ion source.

The NMS parameters are shown in Table IV.

3.1.3. *Helium Abundance Interferometer (HAD)*

PI: U. von Zahn (Bonn), D. M. Hunten (Arizona). Objective: precise (0.1%) determination of the relative abunbdance of helium to hydrogen in the well-mixed lower

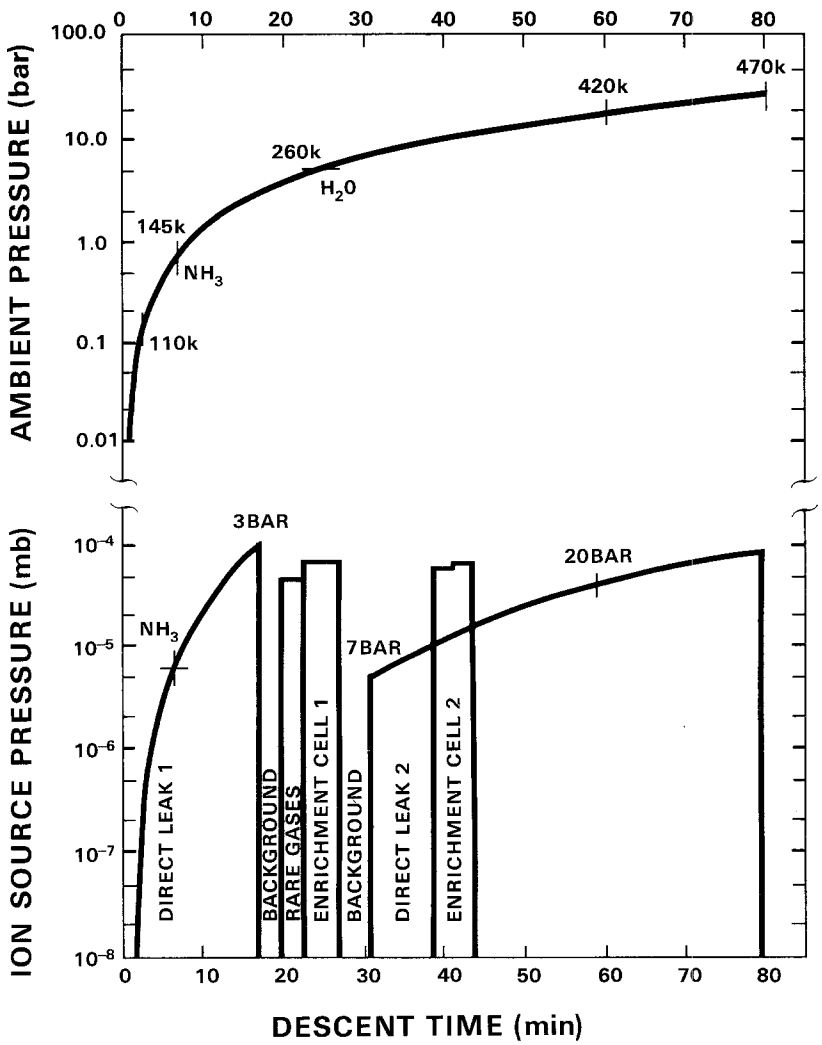

Fig. 8. Measurement program of the Neutral Mass Spectrometer.

atmosphere. Detect variations, if any, over the range 2.5 to 10 bars. Employ the results in Jupiter-related studies (evolution, interior structure, heat balance, thermal radiation spectrum, light elements at megabar pressures), Solar System-related studies (bulk composition of Sun, elemental abundances, evolution), cosmology-related studies (nucleosynthesis, big-bang models of helium).

Concept and approach: He/H_2 will be derived from an *in situ* measurement of the difference in refractive index between a reference gas mixture and the Jupiter atmosphere. The technique is to pass two parallel coherent light beams through identical chambers filled with a Jupiter sample gas and a reference gas of known refractive index maintained at the same pressure. A combiner produces an interference pattern with fringes that are offset by amounts given by refractive index differences. He/H_2 is

calculated directly from the direction and magnitude of the offset. The mixing ratio of two gases in such a binary mixture is determined uniquely, provided the indices are different. The Jupiter atmosphere is a good approximation of a binary gas mixture since other gases are less than 1% of He. H_2O, NH_3, CH_4 are eliminated by a dedicated absorption cell.

Instrument: the interferometer is a Janin–Mascart two-arm, double pathlength optical device. It consists of two chambers for the reference and sample gases held at identical pressure and temperature, beam splitter, combiner, absorption cells, heat exchangers, reference gas storage volume, pressure balance device, pressure and temperature sensors. The two redundant light sources are GaAs LED's operating at 910 nm in a pulsed mode, with an interference filter to produce a narrower bandwidth. An array of nine photodiode detectors measures movement of interferometer fringes. The HAD parameter summary is given in Table V.

TABLE V

Helium abundance interferometer experiment
(HAD)
Parameter summary

- $N(He)/N(H_2)$ precision 0.1% (verified in lab tests)
- Source wavelength 900 nm
- Reference gas: 72% Ne + 28% Ar which has same refractive index as 11% He + 89% H_2
- Filter resolution ±7.5 nm
- No. of samples: 15

3.1.4. *Nephelometer (NEP)*

PI: B. Ragent, D. Colburn, J. B. Pollack (all at Ames Research Center), G. Grams (Georgia Institute of Technology), J. E. Blamont (CNES, France). Objectives: determine vertical extent, structure, and microphysical structure of the clouds of Jupiter. Particle sphericity and absorptivity data will also be derived.

Instrument: the optical unit of the scattering nephelometer contains a forward scatter subunit (transmitter, reflector, receiving assemblies) arranged at four scattering angles (5.5 15, 40, 70°) and a backscatter subunit (transmitter, receiving assemblies) for one angle (177°). Two GaAs solid-state laser diodes operate at a wavelength of 900 nm. Receiving assemblies are solid-state silicon detectors with pre-amplifiers. The mirrors are heated to minimize fogging upon descent through the clouds. The entire optical unit is vented and mounted on an instrument shelf extending out of the Probe radially through an aperture in the skin. A deployment mechanism centers the scattering volume more than 10 cm from the Probe exterior after the heat shield is removed. Calibration targets on the Probe aeroshell are used during cruise and entry phases of mission. Figure 9 illustrates the expected accuracy and resolution of each NEP channel together with various cloud particle models and associated scattering probabilities. Table VI summarizes the NEP parameters.

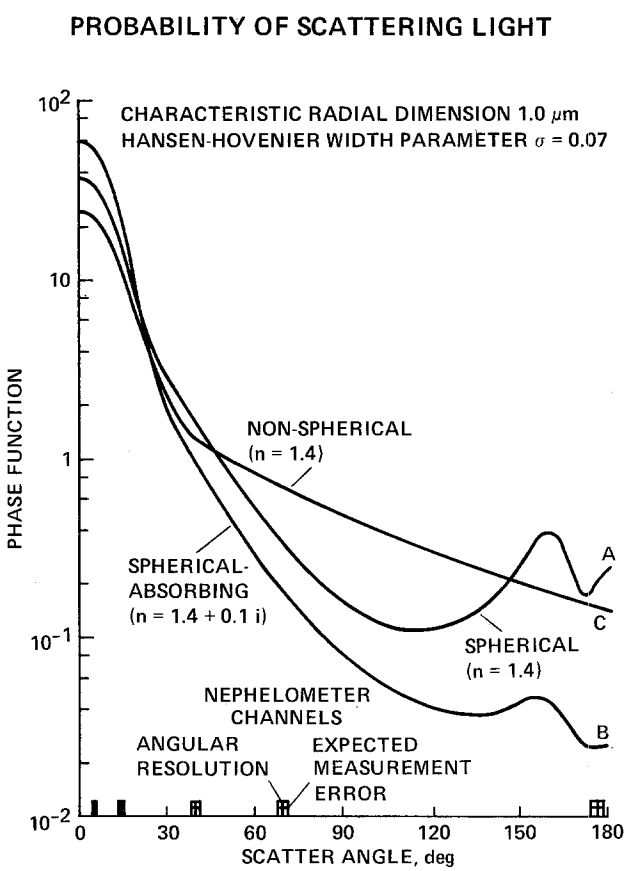

Fig. 9. Probability of scattering light by various particles, with the positions of the Nephelometer channels.

3.1.5. *Net Flux Radiometer (NFR)*

PI: R. W. Boese*, J. B. Pollack, M. Loewenstein (all at Ames Research Center), P. M. Silvaggio (Lawrence Livermore Labs), L. A. Sromovsky* (Wisconsin). Objectives: measure the vertical profile of the difference between the upward and downward going radiation (the net flux) in various spectral regions during Probe descent. Ancillary studies include understanding the planet's radiation budget and atmosphere dynamics, detection of cloud layers and evaluation of their visible and thermal opacity, inference of cloud condensate species, estimating abundance of several trace species that are contributors to atmospheric opacity, provision of 'ground truth' for certain Orbiter experiments, e.g., PPR.

Instrument: multichannel radiometer for alternately viewing the upwelling and downwelling fluxes in 30° cones, $\pm 45°$ from Probe horizontal. Directions not being

* Mr Boese died in December 1985; the new PI will be Dr Sromovsky.

TABLE VI

Nephelometer experiment
(NEP)
Parameter summary

Measurements averaged over altitude intervals of 0.6 km typically. Dynamic range of measurement greater than 10^4 corresponding to visibilities (for Earth-type aerosol concentrations) of greater than 30 km to less than a few meters.

	Minimum sensitivity @ 900 nm
Scattering channel angle	(Scattering cross-section)
5.5 ± 1.0°	3.9×10^{-5} m^{-1} sr^{-1}
15° ± 1.5°	1.1×10^{-5}
40° ± 2.0°	2.4×10^{-6}
70° ± 2.5°	1.0×10^{-6}
177 ± 3.0°	3.5×10^{-7}

Sizing of particles from submicron sizes to greater than 20 μm for particle concentrations greater than a few per cm^3.

viewed are blocked by a shroud for thermal control. A single type 2A diamond window, 9 mm clear aperture, is heated to prevent condensation. The optical system uses a beryllium flat and toroidal focusing mirror. The mirror and condensing cone are coated with a silver surface protected by MgF_2. The detector assembly includes spectral bandpass filters, a six-element lithium tantalate detector array and hybrid pre-amplifiers. All elements, from the window through the detector assembly, are rotated on precision bearings to various positions by a geared stepper motor. Table VII shows the NFR

TABLE VII

NFR spectral bandpasses

Bandpass designation	Nominal spectral bandpass (microns)	Objectives
A	3–500	IR heating rate IR particulate opacity Cloud location
B	0.3–3.5	Solar heating rate Solar particulate opacity Cloud location
C	4.5–5.5	Cloud location (water vapor abundance)
D	14–35	Water vapor abundance
E	0.7–3.5	Methane abundance Cloud location
F	40–105	Ammonia abundance

TABLE VIII

Net flux radiometer
(NFR)
Parameter summary

Optics pointing angle $\pm 45°$ from local horizontal
FOV 40° full cone angle.
Instrument data cycle: twenty 6 s integration periods.
Altitude resolution 1.2 to 0.25 km (6 s integration periods).
Dynamic range $> 10^4$.
Expected performance:

Channel	P (bars)	SNR[a]
A	10	45
B	3	20
C	10	18
D	10	14
E	3	20
F	1.5	30

[a] SNR higher at lower P levels.
NH_3 abundance: better than 2× in range 10 to 0.1 times solar.
H_2O abundance: better than 2× in range 3 to 0.01 times solar.

spectral bandpasses and their relationships to the scientific objectives. Table VIII is a parameter summary for the NFR.

3.1.6. *Lightning and Radio Emission Detector (LRD)*

PI's: L. J. Lanzerotti (Bell Labs and Florida) and K. Rinnert (Max-Planck Institut für Aeronomie, Lindau); G. Dehmel (Technische Universität Braunschweig), F. O. Glein (TUB), E. P. Krider (Arizona), M. A. Uman (Florida).

A second Probe instrument, the Energetic Particles Investigation (EPI), shares the electronics with the LRD. This experiment is described in a companion paper by the Galileo Magnetospheres Working Group.

Objectives: verify the existence of Jovian lightning and provide quantitative data on the Jupiter RF noise spectrum as well as the statistics of the RF pulse amplitudes, widths and spacing and complete RF waveforms. Determine statistics of RF super-bolt occurrences and visible optical impulses from nearly all directions. Waveform data will be acquired with and without optical pulse coincidences according to a priority scheme. From the RF data deduce number and location of lightning cells, scale-size of cloud turbulence, evidence for precipitation, atmospheric vertical static stability, large-scale atmospheric dynamics, and energy content of lightning discharges. Measure inner Jovian magnetosphere at four pre-entry locations (RF noise levels and Jovian magnetic field component perpendicular to the Probe spin axis).

Instrument (Figure 10): three basic sensors: one electromagnetic, two optical. The electromagnetic sensor is a ferrite core antenna, with a linear low-noise pre-amplifier, mounted perpendicular to the Probe spin axis on the equipment cover under the aft heat

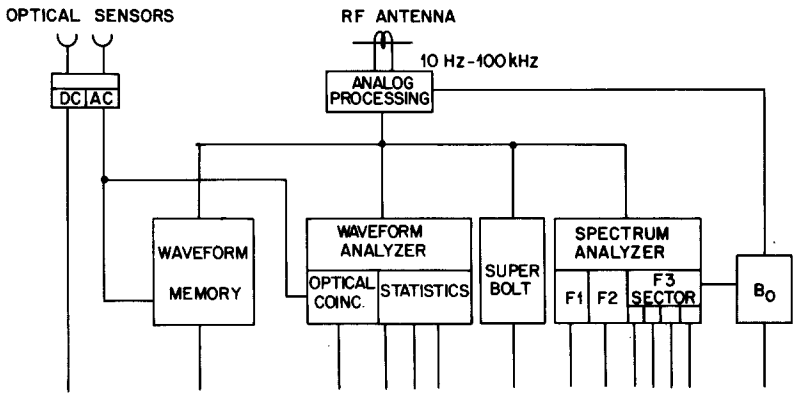

Fig. 10. The lightning detectors of the LRD experiment.

TABLE IX

Lightning and radio emission detector (LRD) Parameter summary

- Lightning detection $\sim 10^4$ km
- Frequency range for waveform measurements and RF pulse statistics ~ 10 Hz to 100 kHz
- Narrow-band, high-sensitivity frequency measurements centered at ~ 3, ~ 15, ~ 90 kHz
- Optical pulse statistics
- Superbolt discharge statistics
- Pulse statistics and RF spectra are accumulated for 4 min intervals, as well as one complete waveform selected by a priority scheme
- Magnetosphere RF frequency measurements ~ 4, 3, 2, 1 R_J altitudes

shield. The optical sensors are two photodiodes behind fisheye lenses which view perpendicular to the Probe spin axis. The two sensors are mounted 180° apart to give the 4π steradian field of view. Table IX is a parameter summary for the LRD.

3.2. The Orbiter

The instantaneous angular fields of view of the atmospheric remote sensing instruments on the Orbiter are compared in Figure 11 and Table X. The spatial resolution and measurement periods for the various instrument modes of operation are also given. More detail appears in the following subsections on each of the Orbiter remote sensing experiments.

3.2.1. *Solid State Imaging System (SSI)*

The Scientific Investigators for the SSI experiment are: Michael J. S. Belton (Team leader, Kitt Peak National Observatory), Clifford D. Anger (Univ. of Calgary, Canada), Michael H. Carr (U.S. Geological Survey, Palo Alto), Clark R. Chapman (Planetary

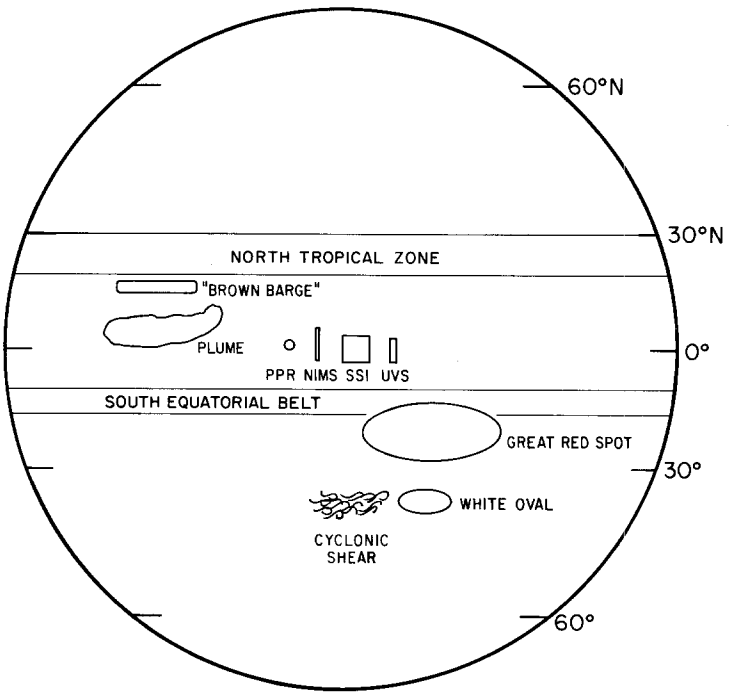

Fig. 11. Sizes of instrumental fields of view for a spacecraft distance of 10 R_J. SSI field-of-view is the frame size (800 × 800 elements). NIMS field-of-view has 20 elements on a line. Size of Jupiter features are appropriate for subspacecraft location.

TABLE X

Spatial and temporal resolutions of atmospheric remote sensing instruments on Galileo Orbiter. The integration time for SSI will be commandable to periods of up to at least tens of seconds. The PPR integration times are also commandable to periods up to 256 times the nominal integration time

Instrument	Instantaneous angular field-of-view		Normal measurement period
			Exposure times
SSI	Frame size		Normal mode 5 ms to 1 s
	(800 × 800 elements)	8 × 8 mrad	
			Time exposure 2 s to tens of s
NIMS	IFOV (rectangular)	0.5 × 10 mrad	
			Spectral scan time: 4.3 s
	pixel size	0.5 × 0.5 mrad	
PPR	IFOV (circular)	2.5 mrad diameter	Cycle mode 19 s
			Photom/polar 13 s
			Photometry 8 s
			Radiometry ≥8 s
			Single position 0.233 s (photom/polar)
			Integration time 0.467 s (radiometry)
UVS	IFOV (rectangular)	1.75 × 7 mrad	Spectral scan time: 4.3 s

Science Institute), Merton E. Davies (Rand Corporation), Ronald Greeley (Arizona State Univ.), Richard Greenberg (University of Arizona), James W. Head (Brown University), Gerhard Neukum (DFVLR, West Germany), Carl B. Pilcher (Univ. of Hawaii), Joseph Veverka (Cornell Univ.), John B. Wellman (Jet Propulsion Laboratory).

The following interdisciplinary Scientists are also closely involved with the experiment: Harold Masursky (U.S. Geological Survey, Flagstaff), David Morrison and Fraser Fanale (Univ. of Hawaii), Peter Gierasch (Cornell Univ.), and Gerald Schubert (Univ. of California, Los Angeles).

Instrument development is the responsibility of the Imaging Systems Division at the Jet Propulsion Laboratory. Mr Kenneth Klaasen is the JPL experiment representative and is responsible for the interface between both the Galileo project and the Imaging Systems Division at JPL and the Scientific Investigator Team.

The SSI camera-telescope utilizes an optical system similar to the narrow-field cameras flown on Voyager and Mariner 10. In the telescope system the following changes were made for Galileo: (1) The anti-reflection and thermal coatings were changed to allow efficient operation at wavelengths longer than 650 nm. The sensitivity range is 400 to 1000 nm. (2) A thick quartz plug has been inserted in the optical path just ahead of the detector to help shield it from magnetospheric radiation. (3) Mechanical baffling of scattered light in the optical system has been modified so that scattered light is greatly reduced.

The camera head is a completely new design and features a 'Virtual Phase Charge-coupled Device', a solid-state detector fabricated by Texas Instruments. The detector is passively cooled to near 163 K and is protected from magnetospheric particle radiation by heavy tantalum shields. Shutter and filter mechanisms are similar to those of previous Mariner class imaging subsystems.

The new detector yields an overall factor of about 100 increase in sensitivity and allows efficient operation at wavelengths between 650 and 1000 nm that were inaccessible to early planetary imaging systems. This extension of spectral range is important for imaging science objectives at Jupiter. Imaging at wavelengths *less* than 400 nm is not possible with this system.

The objectives of the SSI experiment for investigation of Jupiter's atmosphere are:

(a) *Atmospheric energetics.* Separation of atmospheric mass motions from wave motions at global scales. Identification of wave propagation modes and the levels at which they exist. Characterization of atmospheric flow, clouds, wave fields, and the occurrence of lightning.

(b) *Atmospheric structure.* Vertical structure of a few specific types of atmospheric features by center to limb, multispectral imaging. Characterization of the relationship between vertical cloud structure, color, and morphology.

(c) *Atmospheric motions.* Measurement of the mean vertical wind profile through relative cloud motions. This is to be done at the boundary of major belts and zones, in the region of Probe descent and for several specific atmospheric features (provides information on horizontal drives for motions).

(d) *Radiative properties of the atmosphere.* Measure the scattering properties of individual features at several wavelengths and a wide range of phase angles as a contribution to the determination of local energy balance.

(e) *Magnetospheric interactions.* Map and characterize auroral phenomena in the Jovian atmosphere and correlate it with simultaneous particle and field observations.

Table XI summarizes the SSI instrumental characteristics. The SSI will be mounted on the scan platform bore-sighted with the NIMS, PPR, and UVS instruments. Control

TABLE XI

Performance parameters and physical characteristics of SSI

Parameter	Value
Angular resolution	10.16 μr/pixel
Shortest exposure	4.16 ms
Longest exposure	51.2 s
Active CCD area	12.19 × 12.19 mm
Active lines per frame	800
Active pixels per line	800
CCD full well capacity	1×10^5 electrons
Dark current	< 10 elec/s/pixel
Bits/picture element	8 raw
	3.24 compressed
Readout noise per pixel	~30 electrons r.m.s.
Number of filters	8
Gain states	4 (1, 4, 10, 40)
Mass	28 kg
Average power	17 W
Peak power	23 W
Dimensions	L: 90 cm
	W: 25 cm
	H: 30 cm

of the SSI itself includes commandable selection of spectral filter, exposure duration, gain state, image readout rate, data compression, and microcomputer configuration control. Figure 12 shows the seven filter band-passes (there is an eighth clear position) and Figure 13 illustrates the camera-telescope system.

3.2.2. *Near-Infrared Mapping Spectrometer (NIMS)*

The investigators for the NIMS experiment are R. Carlson (Principal Investigator, Jet Propulsion Laboratory), G. E. Danielson (Calif. Inst. Tech.), T. Encrenaz (Obs. de Paris), F. P. Fanale (Univ. of Hawaii), T. V. Johnson (Jet Propulsion Lab.), H. Kieffer, (U.S. Geological Survey), J. S. Lewis (Univ. of Arizona), H. Masursky (USGS), D. L. Matson (Jet Propulsion Lab.), T. B. McCord (Univ. of Hawaii), L. A. Soderblom (USGS), and F. W. Taylor (Univ. of Oxford).

The NIMS experiment uses a grating spectrometer to measure radiances between 0.7 and 5.2 μm with a spectral resolution of 0.025 μm. Images are formed using a line-scan

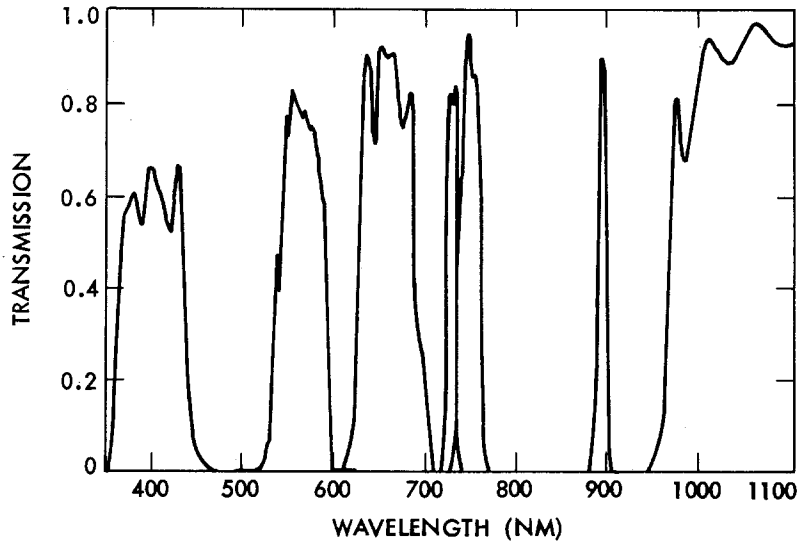

Fig. 12. The filters of the imaging system.

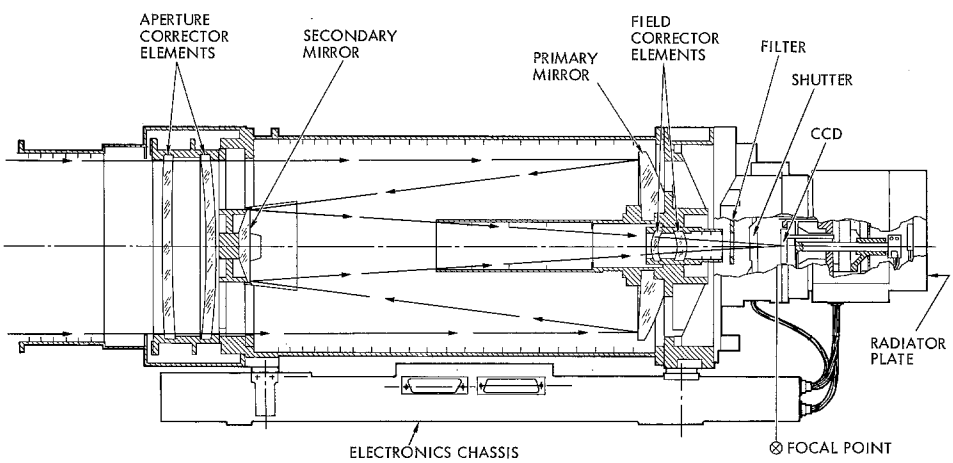

Fig. 13. Cross section of the SSI optical system.

technique. The field of view consists of a line of 20 contiguous 0.5 × 0.5 mrad samples, which will be scanned across the target by means of the spacecraft and scan platform motion.

The NIMS atmospheric science measurements are:

(1) Global distributions and time variability of some minor atmospheric constituents.

(2) Atmospheric temperature in the range from about 1 bar down to the first opaque cloud layer.

(3) Cloud coverage and layering.

TABLE XII

NIMS instrumental characteristics

Parameter	Characteristic
Angular resolution	0.5 mrad × 0.5 mrad
Angular field	10 mrad (20 pixels) × 0.5 mrad (1 pixel)
Spectral range	0.7–5.3 μ
Spectral resolution	0.6%; $\Delta\lambda$ = 0.025 μ ($\lambda > 1$ μ); 0.013 μ ($\lambda < 1$ μ).
Spectral scan time	$4\frac{1}{3}$ seconds (20 pixels, 204 wavelengths).
Telescope	23 cm (9″) diameter *f*/3.5 Ritchey–Chrétien, Wobbling secondary for spatial scan, 800 mm equivalent focal length.
Etendue (AΩ)	1.1×10^{-4} cm^2 sterad.
Spectrometer	40 lines/mm plane-grating spectrometer, *F*/3.5 Dall-Kirkham collimator f = 400 mm, *F*/1.75 wide-angle flat-field camera f = 200 mm.
Detectors	InSb(15), Si(2), discrete elements, Quantum efficiency ≈ 80–80%, Noise Equivalent Power = 10^{14} Watts, D* = 3×10^{13} cm $\sqrt{\text{Hz}}$ Watt^{-1}. Radiatively cooled to 80° K.
Noise equiv. radiance	1.2×10^{-9} W cm^{-2} sterad^{-1} per spectral resolution element (0.025 μ) at 3 μ.
Signal-to-noise	≈ 100:1 (0.075 albedo surface at 3 μ)
Mass	18.0 kg
Power	8 W (average) 12 W (peak)
External dimensions	82.6 × 36.8 × 39.1 cm (optics), 20.3 × 25.4 × 12.7 cm (electronics).
Data rate	11.52 kbps
Date encoding	10 bits

(4) Scattering characteristics of the clouds as a function of solar phase angle and wavelength, and inferences regarding their physical properties and composition.

(5) Imaging of Jupiter at selected infrared wavelengths (e.g., in the 5 μm 'window'), day and night side.

The NIMS instrument characteristics are summarized in Table XII. The instrument (Figure 14) consists of an *f*/3.5 Cassegrain reflector telescope with 800 mm focal length, a grating spectrometer, and a series of detectors in the focal plane. The linear array of detectors has 15 indium antimonide and 2 silicon photodiodes each of which samples a specific wavelength interval, depending on the order and rotation angle of the grating. Optical filters are used to isolate individual orders. The focal plane assembly is radiatively cooled to 75–80 K.

3.2.3. *Photopolarimeter Radiometer (PPR)*

The investigators for the PPR experiment, at the Goddard Institute for Space Studies unless indicated otherwise, are J. E. Hansen (Principal Investigator), M. D. Allison, A. D. Del Genio, A. A. Lacis, G. S. Orton (Jet Propulsion Laboratory), W. B. Rossow, P. H. Stone (Massachusetts Institute of Technology), L. D. Travis, Y. L. Yung (Calif. Inst. of Tech.), and D. Morrison (Univ. of Hawaii).

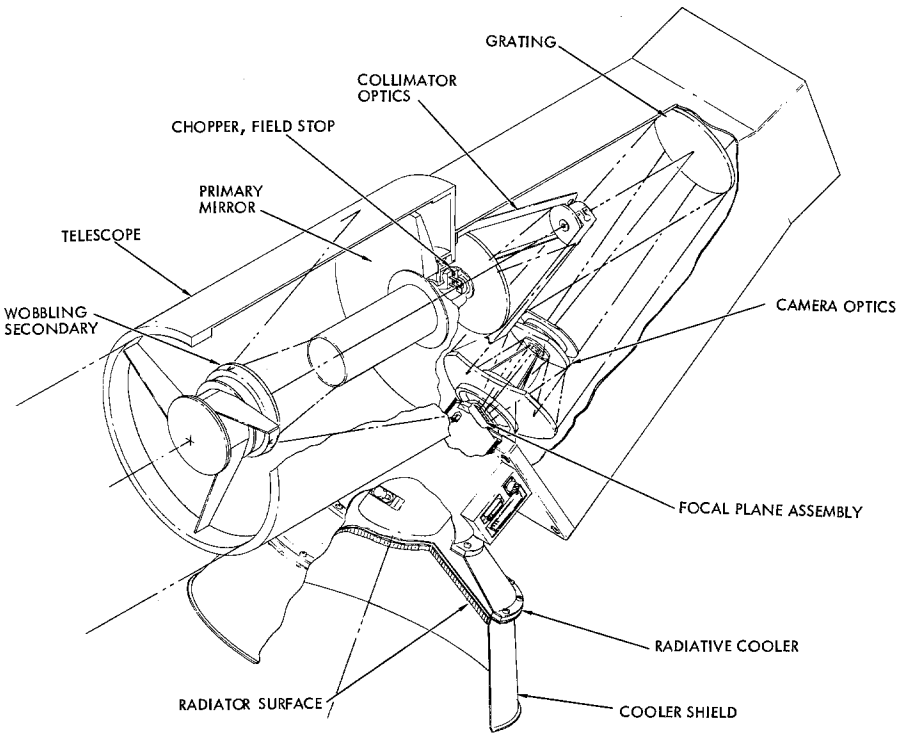

Fig. 14. Pictorial view of basic components of NIMS.

The PPR atmospheric science measurements will be (1) global and regional radiation budget (total solar and total thermal fluxes, and vertical distribution of solar heating), (2) temperature profiles (100–500 mb), and (3) cloud and haze properties (vertical and horizontal distribution and microstructure).

Principal applications of the data will be (1) interpretation and extension of Probe data, for example by placing the radiation, temperature, and cloud particle measurements of the Probe in a global context and by providing boundary conditions above 100 mb where the Probe does not operate, (2) interpretation of the Galileo images of Jupiter by providing information on the atmospheric pressure levels of observed features, as well as cloud and haze properties, temperature profiles and the radiation budget for selected regions, and (3) global Jupiter investigations as discussed in Section 2, particularly those related to the energetics of the general circulation and climate of Jupiter's atmosphere, the magnitude and latitudinal variation of the internal energy source, the physical nature and variability (temporal and spatial) of the cloud and aerosol layers, and the interactions and feedbacks of the clouds and aerosols with the general circulation and climate.

The PPR uses a 10-cm diameter Cassegrain telescope (Figure 15) bore-sighted with the UVS, NIMS, and SSI instruments on the scan platform. The 32-position filter wheel (Figure 16) permits photometric, polarimetric, and radiometric measurements (radiation

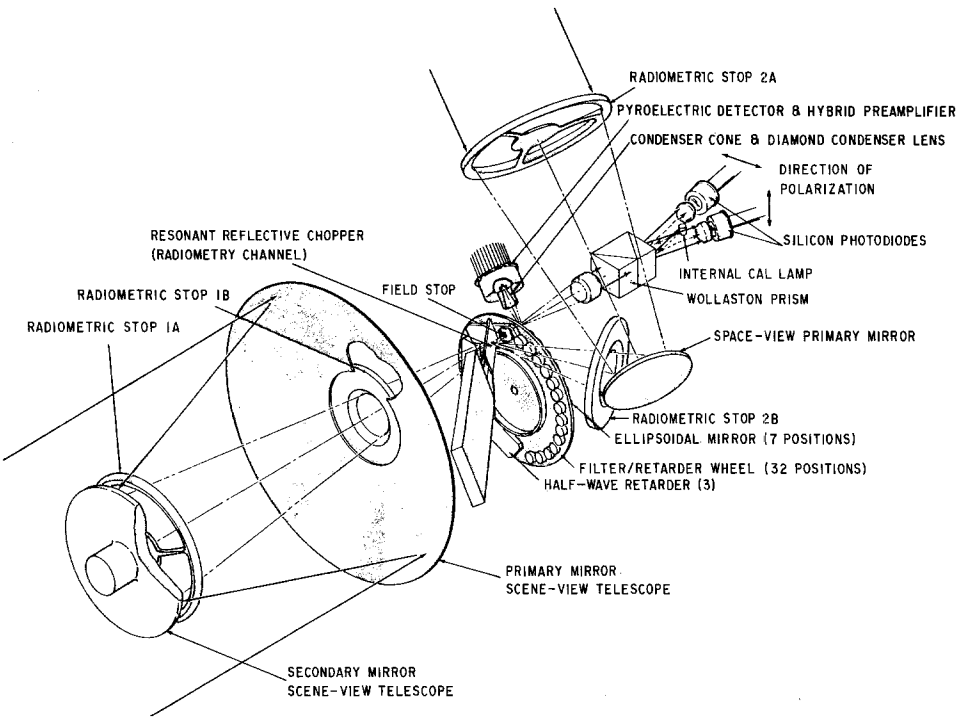

Fig. 15. Pictorial view of PPR optical system.

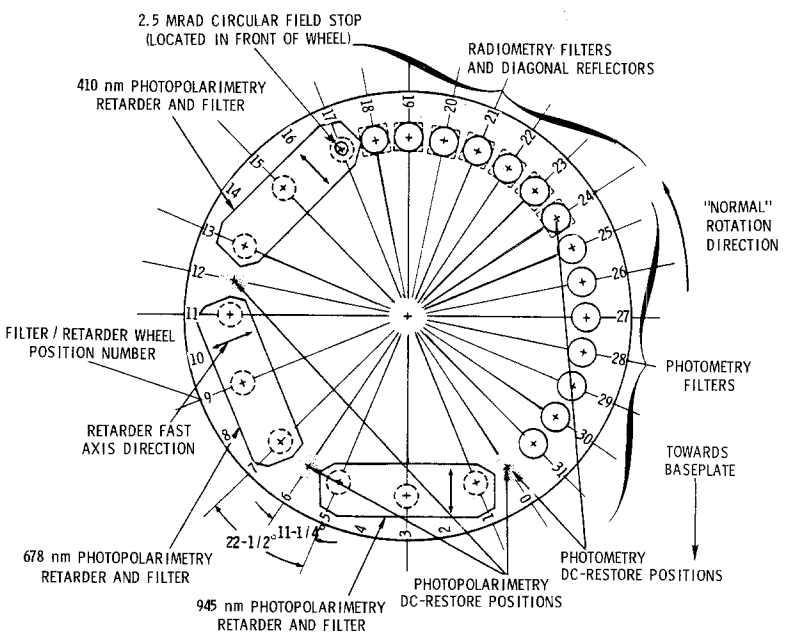

Fig. 16. PPR filter/retarder wheel layout.

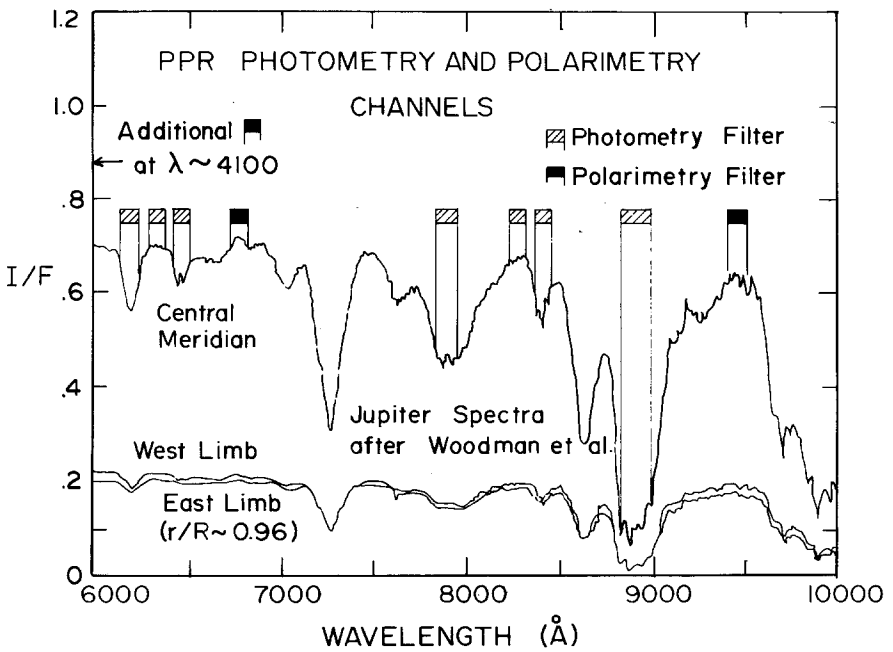

Fig. 17. Spectral locations of PPR photometry and polarimetry channels.

budget and the flux in filtered thermal bands) in series. A 2.5 m fixed circular field stop in front of the filter wheel defines the field-of-view. A resonant reflective chopper provides alternate viewing of the scene and space. Calibration, in addition to the space view port, is provided by internal and external inflight calibrator lamps and by external photometric and radiometric calibration targets which can also be viewed by NIMS, SSI, and UVS.

The spectral locations of the PPR photometry and polarimetry channels are shown in Figure 17 and the approximate locations of the filtered thermal bands in Figure 18. The instrument parameter summary is given in Table XIII. The PPR can operate in any

TABLE XIII

PPR instrumental characteristics

Field of view	2.5 mrad (circular)
Detectors	Polarimetry and photometry: silicon photodiode Radiometry: Lithium tantalate pyroelectric
Spectral bands	Polarimetry: 410, 678, and 945 nm Photometry: 618, 633, 646, 789, 830, 841, and 892 nm Radiometry: 17, 21, 28, and 36 μm; $\lambda \geq 42$ μm; Solar ($\lambda < 4$ μm); Solar plus thermal (no filter)
Telescopes	10 cm diameter $f/5$ Cassegrain for scene view; plane mirror space view
Mass	5.0 kg
Power	4.5 W (average); 9 W (peak)
Size	45 × 19 × 33 cm
Data rate	216 bps

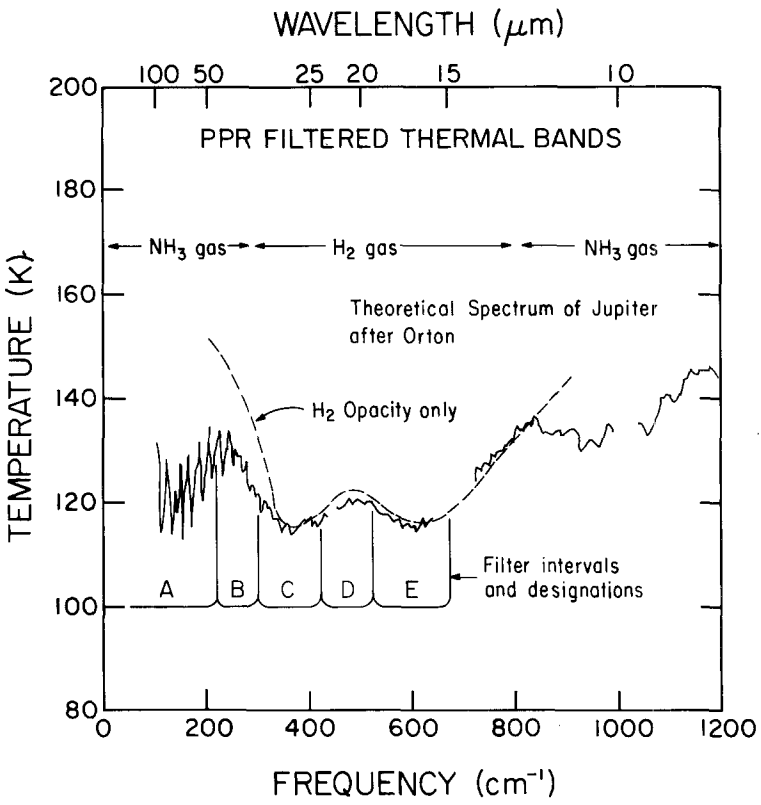

Fig. 18. Approximate spectral locations of PPR filtered thermal bands.

of several modes: (1) cycle mode (all 32 filter wheel positions consecutively), (2) polarimetry plus photometry, (3) photometry, (4) radiometry, and (5) position select (any one of 32 positions).

3.2.4. *Ultraviolet Spectrometer (UVS)*

The investigators for the UVS experiment, all at the University of Colorado unless indicated otherwise, are: C. W. Hord (Principal Investigator), C. A. Barth, G. E. Thomas, A. I. Stewart, and A. L. Lane (Jet Propulsion Laboratory).

The UVS experiment uses an Ebert–Fastie spectrometer to measure radiance in the 115–430 nm range with a resolution of approximately 1 nm. The UVS rectangular (1.85 × 7 mrad) field of view in the preferred observational mode will be oriented parallel to the planetary limb and scanned across (and off) the disk from limb-to-limb. Observations of both the day side and night side of Jupiter are intended.

The principal objectives of the UVS experiment for investigation of Jupiter's atmosphere are:

(a) *Stratospheric composition.* The spatial distribution and temporal variability of NH_3, hydrocarbons and other UV-active molecules will be studied. There will be a

search for regions where complex molecules are being formed, e.g., by photodissociation by UV sunlight or charged-particle bombardment, with special attention to certain locations on the planet, such as the polar regions and the Great Red Spot.

(b) *Upper atmospheric atomic and molecular hydrogen.* The abundance of H and H_2 above the homopause will be determined, and the temporal and spatial variations of the H_2 abundance (or, effectively, variations in the homopause pressure level) will be sought.

(c) *Auroral phenomena.* Ultraviolet emissions from the dark side of the planet will be measured. It is expected that the helium abundance can be determined at the level of charged particle penetration. It is also expected that a morphological description of the coupling of Jupiter's magnetosphere with the atmosphere can be obtained.

(d) *Cloud and haze structure.* Vertical optical depth unity for Rayleigh scattering from H_2 + He occurs in the 130–770 mbar region for the spectral range 200–300 nm. Continuum spectral reflectivity measurements across the disk in the near-UV will provide constraints on the vertical and horizontal distribution of chromophores in the upper troposphere and stratosphere.

(e) *Satellites.* Bright and dark limb scans will be used to measure and set upper limits on escape rates of volatiles from satellite surfaces. Electron impact and/or solar excitation of atoms such as hydrogen and oxygen will provide a sensitivity of 10 to 10 000 atoms cm^{-3} depending on the species.

The areal distribution of absorbers such as sulfur dioxide will be mapped on the satellite surfaces.

The UVS instrument (Table XIV) consists of a telescope-spectrometer with three detectors. The Cassegrain telescope has a 5 cm primary mirror and a 250 mm focal length. The spectrometer grating has 2400 lines per mm and may be used in a fixed position or moved continuously to cover the spectral range. The spectrometer has three exit slits with the dispersed light from each imaged on a detector. The three detectors have three separate photocathode surfaces which give three independent spectral channels. The short wavelength (WG) channel has an 0.1 × 1.4° field of view, ~0.7 nm resolution (FWHM), and measures the radiance between 115 and 180 nm diffracted in

TABLE XIV

UVS instrumental characteristics

Parameter	Characteristic
Mass	4.2 kg
Power	4.2 watts
Dimensions	16 × 6 × 6 in. (L × W × H)
Data rate	1008 bps
Spectral resolution	7 Å, 1150 to 1800 Å: 2nd order
	13 Å, 1600 to 4300 Å; 1st order
Spectral range	1150 to 4300 Å
Fields of view	0.1° × 1.4°, 1150–1800 Å and 2800–4300 Å
	0.1° × 0.4°, 1600 – 3000 Å
Spectral scan time	4.3 s

second order. At 130 nm the sensitivity is ~ 500 counts per second per kiloRayleigh [1 Rayleigh = 10^6 photons cm^{-2} s^{-1} $(4\pi$ sterad$)^{-1}$]. The second (F) channel has a $0.1 \times 0.4°$ field of view, ~ 1.3 nm resolution, and measures the radiance from 280 to 430 nm in first order. The observations of Jupiter will be made primarily with the G- and F-detectors. The electronics concept for the instrument is similar to that of the Pioneer Venus UV spectrometer (Colin and Hunten, 1977). A command capability allows flexibility in grating position and accumulation times for the different channels.

3.3. Radio Science Investigations

The Galileo radio telecommunication system provides the opportunity for several science investigations. The Radio Science (RS) investigations will be carried out by two teams: the Celestial Mechanics and Relativity team composed of J. Anderson (team leader) and Frank Estabrook, and the Radio Propagation team composed of H. T. Howard (team leader, Stanford), V. Eshleman (Stanford), A. Kliore, G. Lindal, and R. Woo. All are at the Jet Propulsion Laboratory unless indicated otherwise.

Investigators will use the signals transmitted between the Earth and the orbiter and between the Probe and the Orbiter to carry out their investigations. Earth–Orbiter communications will use an S-band (2115 MHz) uplink (Earth-spacecraft) and transponder to generate a coherent S–X band (2297 and 8422 MHz) downlink, using an Earth-oriented 5 m dish antenna. Frequency stability is ~ 1 part in 10^{11}. Probe-to-Orbiter transmission will be at a frequency of 1387 MHz, to a wide-band receiver and body-fixed 1 m dish antenna.

Atmospheric investigations using radio techniques are:

S–X band occultations (Eshleman, Kliore, Lindal). Measure pressure, temperature, and absorptivity profiles of the troposphere and lower stratosphere. Measure electron density profiles in the ionosphere.

Scintillations (Woo, Eshleman). Deduce (1) turbulence in the lower atmosphere; (2) electron density irregularities, magnetic field direction, and winds in the ionosphere.

Probe–Orbiter doppler shifts (Kliore; also Interdisciplinary Scientists Pollack, Gierasch). Use the horizontal component of Probe motion to deduce zonal wind speeds from 100 mb to 10–20 bars. Accurately locate the Probe entry site.

S-band Faraday rotation (Howard). Measure magnetic fields near the cloud tops and up into the magnetosphere.

3.4. Interdisciplinary Scientist Investigations

Nine of the Interdisciplinary Scientists chosen to participate in the Galileo mission will perform investigations pertinent to the Jovian atmosphere: P. J. Gierasch (Cornell), D. M. Hunten (Arizona), A. P. Ingersoll (CIT), M. B. McElroy (Harvard), G. S. Orton (JPL), T. C. Owen (SUNY), J. B. Pollack (ARC), C. Sagan (Cornell), and G. Schubert (UCLA). Their intended investigations can be summarized in the following categories:

Dynamics (Gierasch, Ingersoll, Pollack, Schubert). Nature of, and driving forces for, the visible circulation and its extension to the greatest possible depth. Evolution of the planet since its formation.

Composition (Hunten, McElroy, Owen, Sagan). Basic analysis of components present. Interpretation of non-equilibrium compounds in terms of photochemistry, transport from other parts of the atmosphere, and lightning. Cosmological and cosmogenical implications. Organic compounds and cloud coloration.

Structure, thermal radiation (Orton, Pollack, Hunten). Establishment of the basic temperature profile and interpretation of its deviations from simple models. Heat flow and its implications. Cloud and haze layers.

Satellite Atmospheres (McElroy, Hunten). Existence, compositions, sources, sinks, and energy balance.

References

Allison, M. D.: 1983, 'Planetary Waves in Jupiter's Equatorial Atmosphere', *Bull. Am. Astron. Soc.* **15**, 836.

Allison, M. D., and Gierasch, P. J.: 1982, 'Jovian Atmospheric Dynamics: Global-Scale Motion and Shear Instability for a Thin, Nearly Adiabatic Upper Weather Layer', *Bull. Am. Astron. Soc.* **14**, 722.

Allison, M. D., and Gierasch, P. J.: 1984, 'Jovian Meteorology: Large-Scale Motion in a Thin, Weakly Stratified Weather Layer with Convective Forcing', unpublished draft.

Appleby, J. F. and Hogan, J. S.: 1984, 'Radiative-Convective Equilibrium Models of Jupiter and Saturn', *Icarus* **59**, 336.

Axel, L.: 1972, 'Inhomogeneous Models of the Atmosphere of Jupiter', *Astrophys. J.* **173**, 451.

Bezard, B., Baluteau, J. P., and Marten, A.: 1983, 'Study of the Deep Cloud Structure in the Equatorial Region of Jupiter from Voyager Infrared and Visible Data', *Icarus* **54**, 434.

Bjoraker, G., Fink, U., Larson, H. P., and Kunde, V.: 1981, 'H_2O and PH_3 Abundances from 5 μm Measurements', *Bull. Am. Astron. Soc.* **13**, 735.

Bjoraker, G. L., Larson, H. P., and Kunde, V. G.: 1986a, 'The Gas Composition of Jupiter Derived from 5-μm Airborne Spectroscopic Observations', *Icarus* **66**, 579.

Bjoraker, G. L., Larson, H. P., and Kunde, V. G.: 1986b, 'The Abundance and Distribution of Water Vapor in Jupiter's Atmosphere', *Astrophys. J.* **311**, 1058.

Bragg, S. L., Brault, J. W., and Smith, W. H.: 1982, 'Line Positions and Strengths in the H_2 Quadrupole Spectrum', *Astrophys. J.* **263**, 999.

Broadfoot, A. L., Sandel, B. R., Shemansky, D. E., McConnell, J. C., Smith, G. R., Holberg, J. B., Atreya, S. K., Donahue, T. M., Strobel, D. F., and Bertaux, J. L.: 1981, 'Overview of the Voyager Ultraviolet Spectrometry Results through Jupiter Encounter', *J. Geophys. Res.* **86**, 8259.

Buriez, J. C. and de Bergh, C.: 1980, 'Methane Line Profile near 1.1 μ as a Probe of the Jupiter Cloud Structure and C/H Ratio', *Astron. Astrophys.* **83**, 149.

Busse, F. H.: 1983, 'A Model of Mean Zonal Flows in the Major Planets', *Geophys. Astrophys. Fluid Dynamics* **23**, 153.

Caldwell, J., Cess, R. D., and Carlson, R. E.: 1979, 'Temporal Characteristics of the Jovian Atmosphere', *Bull. Am. Astron. Soc.* **11**, 587.

Caldwell, J., Tokunaga, A. T., and Orton, G. S.: 1981, 'Further Observations of 8 μm polar brightenings on Jupiter', *Icarus* **53**, 133.

Cameron, A. G. W. and Pollack, J. B.: 1976, 'On the Origin of the Solar System and of Jupiter and its Satellites', in T. Gehrels (ed.), *Jupiter*, Tucson, University of Arizona Press, pp. 61–84.

Clark, P., French, R., and Gierasch, P.: 1979, 'Voyager IRIS thermal data: Theory of Stratospheric Waves', *Bull. Am. Astron. Soc.* **11**, 587.

Coffeen, D. L.: 1974, 'Optical Polarization Measurements of the Jupiter Atmosphere at 103° Phase Angle', *J. Geophys. Res.* **79**, 3645.

Colin, L. and Hunten, D. M.: 1977, 'Pioneer Venus Experiment Descriptions', *Space Sci. Rev.* **20**, 451.

Conrath, B. J. and Gierasch, P. J.: 1984, 'Global Variation of the Para Hydrogen Fraction in Jupiter's Atmosphere and Implications for Dynamics on the Outer Planets', *Icarus* **57**, 184.

Conrath, B. J., Gierasch, P. J. and Nath, N.: 1981, 'Stability of Zonal Flows on Jupiter', *Icarus* **48**, 256.

Cook, A. F., Duxbury, T. C., and Hunt, G. E.: 1979a, 'A Lower Limit on the Top of Jupiter's Haze Layer', *Nature* **280**, 780.

Cook, A. F., Duxbury, T. C., and Hunt, G. E.: 1979b, 'First Results on Jovian Lightning', *Nature* **280**, 794.
Drossart, P., Encrenaz, T., Kunde, V., Hanel, R., and Combes, M.: 1982, 'An Estimate of the PH_3, CH_3D, and GeH_4 Abundances on Jupiter from the Voyager IRIS Data at 4.5 μm', *Icarus* **49**, 416.
Encrenaz, T. and Combes, M.: 1982, 'On the C/H and D/H Ratios in the Atmospheres of Jupiter and Saturn', *Icarus* **52**, 54.
Fanale, F. P., Banerdt, W. B., Elson, L. S., Johnson, T. V., and Zurek, R. W.: 1982, in D. Morrison (ed.), 'Io's surface: Its Phase Composition and Influence on Io's Atmosphere and Jupiter's Magnetosphere', *The Satellites of Jupiter*, University of Arizona Press, Chap. 20.
Flasar, F. M., Conrath, B. J., Pirraglia, J. A., Clark, P. C., French, R. G., and Gierasch, P. J.: 1981, 'Thermal Structure and Dynamics of the Jovian Atmosphere, I. The Great Red Spot', *J. Geophys. Res.* **86**, 8759.
Frank, L. *et al.*: 1987, *Space Sci. Rev.*, to be published.
Gautier, D., Bezard, B., Marten, A., Baluteau, J. P., Scott, N., Chedin, A., Kunde, V., and Hanel, R.: 1982, 'The C/H Ratio in Jupiter from the Voyager Infrared Investigation', *Astrophys. J.* **257**, 901.
Gautier, D. and Owen, T.: 1983a, 'Cosmological Implications of Helium and Deuterium Abundances on Jupiter and Saturn', *Nature* **302**, 215.
Gautier, D. and Owen, T.: 1983b, 'Cosmological Implications of Elemental and Isotopic Abundances in Atmospheres of the Giant Planets', *Nature* **304**, 691.
Gautier, D., Bezard, B., Marten, A., Baluteau, J. P., Scott, N., Chedin, A., Kunde, V., and Hanel, R.: 1982, 'The C/H Ratio in Jupiter from the Voyager Infrared Investigation', *Astrophys. J.* **257**, 901.
Gierasch, P. J.: 1976, 'Jovian Meteorology: Large-Scale Moist Convection', *Icarus* **29**, 445.
Gierasch, P. J.: 1983, 'Dynamical Consequences of Orthohydrogen-Parahydrogen Disequilibrium on Jupiter and Saturn', *Science* **219**, 847.
Gillett, F. C., Low, F. J., and Stein, W. A.: 1969, 'The 2.8–1.4 Micron Spectrum of Jupiter', *Astrophys. J.* **157**, 925.
Gulkis, S. and Poynter, R.: 1972, 'Thermal Radio Emission from Jupiter and Saturn', *Phys. Earth Planet. Interiors* **6**, 36–43.
Gurnett, D. A., Shaw, R. R., Anderson, R. R., Kurth, W. S., and Scarf, F. L.: 1979, 'Whistlers Observed by Voyager 1: Detection of Lightning on Jupiter', *Geophys. Res. Letters* **6**, 511.
Hanel, R., Conrath, B., Herath, L., Kunde, V., and Pirraglia, J.: 1981, 'Albedo, Internal Heat, and Energy Balance of Jupiter: Preliminary Results of the Voyager Infrared Investigation', *J. Geophys. Res.* **86**, 8705.
Hanel, R. and 12 co-authors: 1979a, 'Infrared Observations of the Jovian System from Voyager 1', *Science* **204**, 972.
Hanel, R. and 14 co-authors: 1979b, 'Infrared Observations of the Jovian System from Voyager 2', *Science* **206**, 952.
Hord, C. W. and 6 co-authors: 1979, 'Photometric Observations of Jupiter at 2400 Angstroms', *Science* **206**, 956.
Hunt, G. E., Conrath, B., and Pirraglia, J.: 1981, 'Visible and Infrared Observations of Jovian Plumes During the Voyager Encounter', *J. Geophys. Res.* **86**, 8777.
Hunten, D. M. and Veverka, J.: 1976, 'Stellar and Spacecraft Occultation by Jupiter: A Critical Review of Derived Temperature Profiles', in T. Gehrels (ed.), *Jupiter*, University of Arizona Press, Tucson, 247–283.
Ingersoll, A. P.: 1976, 'The Atmosphere of Jupiter', *Space Sci. Rev.* **18**, 603.
Ingersoll, A. P. and Pollard, D.: 1982, 'Motion in the Interiors and Atmospheres of Jupiter and Saturn: Scale Analysis, Anelastic Equations, Barotropic Stability Criterion', *Icarus* **52**, 62.
Ingersoll, A. P. and Porco, C. C.: 1978, 'Solar Heating and Internal Heat Flow on Jupiter', *Icarus* **35**, 27.
Ingersoll, A. P., Beebe, R. F., Mitchell, J. L., Garneau, G. W., Yagi, G. M., and Muller, J.: 1981, 'Interactions of Eddies and Mean Zonal Flow on Jupiter as Inferred from Voyager 1 and 2 Images', *J. Geohpys. Res.* **86**, 8733.
Ingersoll, A. P., Munch, G., Neugebauer, G., and Orton, G. S.: 1976, 'Results of the Infrared Radiometer Experiment on Pioneers 10 and 11', in T. Gehrels (ed.), *Jupiter*, University of Arizona Press, Tucson, 197–205.
Keay, C. S. L., Low, F. J., Rieke, G. H., and Minton, R. B.: 1973, 'High-Resolution Maps of Jupiter at Five Microns', *Astrophys. J.* **183**, 1063.
Kim, S. J., Caldwell, J., Rivolo, A. R., Wagener, R., and Orton, G. S.: 1985, 'Infrared Solar Brightenings on Jupiter III. Spectrometry from the Voyager 1 IRIS Experiment', *Icarus* **64**, 233.
Kliore, A. J., Fjeldbo, G., Seidel, B. L., Sweetnam, D. N., Sesplaukis, T. T., and Woiceshyn, P. M.: 1975, 'The Atmosphere of Io from Pioneer 10 Radio Occultation Measurements', *Icarus* **24**, 407.

Knacke, R. F., Kim, S. J., Ridgway, S. T., and Tokunaga, A. T.: 1982, 'The Abundances of CH_4, CH_3D, NH_3, and PH_3 in the Troposphere of Jupiter Derived from High-Resolution 1100–1200 cm^{-1} Spectra', *Astrophys. J.* **262**, 388.

Kumar, S.: 1982, 'Photochemistry of SO_2 in the Atmosphere of Io and Implications on Atmospheric Escape', *J. Geophys. Res.* **87**, 1677.

Kumar, S. and Hunten, D. M.: 1982, 'The Atmospheres of Io and Other Satellites', in D. Morrison (ed.), *The Satellites of Jupiter*, University of Arizona Press, Chap. 21.

Kunde, V., Hanel, R., Maguire, W., Gautier, D., Baluteau, J. P., Marten, A., Chedin, A., Husson, N., and Scott, N.: 1982, 'The Tropospheric Gas Composition of Jupiter's North Equatorial Belt (NH_3, PH_3, CH_3D, GeH_4, H_2O) and the Jovian D/H Isotopic Ratio', *Astrophys. J.* **263**, 443.

Lacis, A. A. and Hansen, J. E.: 1974, 'Atmosphere of Venus: Implications of Venera 8 Sunlight Measurements', *Science* **184**, 979.

Lanzerotti, L. J., Rinnert, K., Krider, E. P., Uman, M. A., Dehmel, G., Gliem, F. O., and Axford, W. I.: 1983, in L. H. Ruhunke and J. Latham (eds.), *Planetary Lightning and Lightning Measurements on the Galileo Probe to Jupiter's Atmosphere*, Proc. Atmos. Electricity, Deepak Publ. Co., p. 411.

Larson, H. P., Fink, U., Treffers, R. R., and Gautier, T. N.: 1975, 'Detection of Water Vapor on Jupiter', *Astrophys. J.* **197**, L137.

Lebofsky, L. A.: 1974, 'Chemical Composition of Saturn's Rings and Icy Satellites', Doctoral dissertation, Massachusetts Institute of Technology, Cambridge, Mass.

Lewis, J. S.: 1969a, 'The Clouds of Jupiter and the NH_3–H_2O and NH_3–H_2S Systems', *Icarus* **10**, 365.

Lewis, J. S.: 1969b, 'Observability of Spectroscopically Active Compounds in the Atmosphere of Jupiter', *Icarus* **10**, 393.

Lewis, J. S. and Prinn, R. G.: 1970, 'Jupiter's Clouds: Structure and Composition', *Science* **169**, 472.

Lewis, J. S., and Prinn, R. G.: 1971, in A. Schwartz (ed.), 'Chemistry and Photochemistry of the Atmosphere of Jupiter', *Theory and Experiment in Exobiology*, Wolters–Noordhoff, Groningen, Netherlands, pp. 123–142.

Limaye, S. S., Revercomb, Sromovsky, L. A., Krauss, R. J., Santek, D. A., and Suomi, V. E.: 1982, 'Jovian Winds from Voyager 2. Part I: Zonal Mean Circulation', *J. Atmos. Sci.* **39**, 1413.

Lindal, G. F., Wood, G. E., Levy, G. S., Anderson, J. D., Sweetnam, D. N., Hotz, H. B., Buckles, B. J., Holmes, D. P., Doms, P. E., Eshleman, V. R., Tyler, G. L., and Croft, T. A.: 1981, 'The Atmosphere of Jupiter: An Analysis of the Voyager Radio Occultation', *J. Geophys. Res.* **86**, 8721.

Marten, A., Courtin, R., Gautier, D., and Lacombe, A.: 1980, 'Ammonia Vertical Density Profiles in Jupiter and Saturn from Their Radio-Electric and Infrared Emissivities', *Icarus* **41**, 410.

McConnell, J. C., Holberg, J. B., Smith, G. R., Sandel, B. R., Shemansky, D. E., and Broadfoot, A. L.: 1982, 'A New Look at the Ionosphere of Jupiter in Light of the UVS Occultation Results', *Planetary Space Sci.* **30**, 151.

Oort, A. H., and Vonder Haar, T. H.: 1976, 'On the Observed Annual Cycle in the Ocean-Atmosphere Heat Balance over the Northern Hemisphere', *J. Phys. Ocean.* **6**, 781.

Orton, G. S.: 1977, 'Recovery of the Mean Jovian Temperature Structure from Inversion of Spectrally Resolved Thermal Radiance Data', *Icarus* **32**, 41.

Orton, G. S. and Ingersoll, A. P.: 1976, 'Pioneer 10 and 11 and Ground-Based Infrared Data on Jupiter: The Thermal Structure and He–H_2 Ratio', in T. Gehrels (ed.), *Jupiter*, University of Arizona Press, Tucson, pp. 206–215.

Orton, G. S., Appleby, J. F., and Martonchik, J. V.: 1982, 'The Effect of Ammonia, Ice Clouds in the Atmosphere of Jupiter on Outgoing Thermal Radiation', *Icarus* **52**, 94.

Owen, T.: 1969, 'The Spectra of Jupiter and Saturn in the Photographic Infrared', *Icarus* **10**, 355.

Pearl, J., Hanel, R., Kunde, V., Maguire, W., Fox, K., and Gupta, S.: 1979, 'Identification of Gaseous SO_2 and New Upper Limits for Other Gases on Io', *Nature* **280**, 755.

Pirraglia, J. A., Conrath, B. J., Allison, and Gierasch, P. J.: 1981, 'Thermal Structure and Dynamics of Saturn and Jupiter', *Nature* **292**, 677.

Prinn, R. G. and Lewis, J. S.: 1975, 'Phosphine on Jupiter and Implications for the Great Red Spot', *Science* **190**, 274.

Prinn, R. G. and Owen, T.: 1976, 'Chemistry and Spectroscopy', in T. Gehrels (ed.), *Jupiter*, University of Arizona Press, Tucson, pp. 319–371.

Reeves, H., Audouze, J., Fowler, W. A., and Schramm, D. N.: 1973, 'On the Origin of Light Elements', *Astrophys. J.* **179**, 909.

Rinnert, K.: 1983, 'Lightning within Planetary Atmospheres', in H. Volland (ed.), *CRC Handbook of Atmospheric Science,* CRC Press, Boca Raton, Florida.

Rinnert, K., Lanzerotti, L. J., Dehmel, G., Gliem, F. O., Krider, E. P., and Uman, M. A.: 1984: 'RF and Optical Measurements of Jupiter Lightning on the Galileo Jupiter Probe', *Proc. 7th Inter. Conf. Atmos. Electr.*, Am. Meteor. Soc., June.

Rinner, K., Lanzerotti, L. J., Krider, E. P., Uman, M. A., Dehmel, G., Gliem, F. O., and Axford, W. I.: 1979, 'Electromagnetic Noise and Radio Wave Propagation Below 100 kHz in the Jovian Atmosphere, 1, The Equatorial Region', *J. Geophys. Res.* **84**, 5181.

Ross, J. E. and Aller, L. H.: 1976, 'The Chemical Composition of the Sun', *Science* **191**, 1223.

Sato, M. and Hansen, J. E.: 1979, 'Jupiter's Atmospheric Composition and Cloud Structure Deduced from Absorption Bands in Reflected Sunlight', *J. Atmos. Sci.* **36**, 1133.

Sill, G. T.: 1976, 'The Chemistry of the Jovian Cloud Colors', in T. Gehrels (ed.), *Jupiter*, University of Arizona Press, Tucson, pp. 372–383.

Smith, P. H. and Tomasko, M. G.: 1984, 'Photometry and Polarimetry of Jupiter at Large Phase Angles. II. Polarimetry of the South Tropical Zone, South Equatorial Belt, and the Polar Regions from the Pioneer 10 and 11 Missions', *Icarus* **58**, 35.

Smith, D. W., Greene, T. F., and Shorthill, R. W.: 1977, 'The Upper Jovian Atmosphere Aerosol Content Determined from a Satellite Eclipse Observation', *Icarus* **30**, 697.

Smith, B. A. and 10 co-authors: 1977, 'Voyager Imaging Experiment', *Space Sci. Rev.* **21**, 103.

Smith, B. A. and 21 co-authors: 1979a, 'The Jupiter System through the Eyes of Voyager 1', *Science* **204**, 951.

Stoll, C. and Tomasko, M. G.: 1979, 'Jupiter's Atmosphere: Constraints on Scattering Particles from Polarization Measurements', *Bull. Am. Astron. Soc.* **11**, 588.

Stone, P. H.: 1972, 'A Simplified Radiative-Dynamical Model for the Static Stability of Rotating Atmospheres', *J. Atmos. Sci.* **29**, 405.

Stone, P. H.: 1976, 'The Meteorology of the Jovian Atmosphere', in T. Gehrels (ed.), *Jupiter*, University of Arizona Press, Tucson, pp. 586–618.

Terrile, R. J.: 1978, 'High Spatial Resolution Infrared Imaging of Jupiter: Implications for the Vertical Cloud Structure from Five-Micron Measurements', Ph.D. Thesis, California Institute of Technology, Pasadena, 143 pp.

Terrile, R. J. and Westphal, J. A.: 1977, 'The Vertical Cloud Structure of Jupiter from 5 μm Measurements', *Icarus* **30**, 274.

Terrile, R. J., Becklin, E. E., Capps, R. W., and Cruikshank, D. P.: 1979, 'Ground-Based Infrared Imaging of Jupiter During the Voyager Encounters', *Bull. Am. Astron. Soc.* **11**, 586.

Terrile, R. J., Taylor, F. W., and Beer, R.: 1978, 'New Models of the Clouds of Jupiter from Radiometry and Spectrometry in the 5 Micron Spectral Window', *Bull. Am. Astron. Soc.* **10**, 562.

Tomasko, M. G., Clements, A. E., and Castillo, N. D.: 1974, Limb Darkening of Two Latitudes of Jupiter at Phase Angles of 34° and 109°, *J. Geophys. Res.* **79**, 3653.

Tomasko, M. G., West, R. A., and Castillo, N. D.: 1978, 'Photometry and Polarimetry of Jupiter at Large Phase Angles. I. Analysis of Imaging Data of a Prominent Belt and a Zone from Pioneer 10', *Icarus* **33**, 558.

Trauger, J. T., Roesler, F. L., and Mickelson, M. E.: 1977, Paper presented at 32nd Symp. on Molecular Spectrosc., June 13–17, Ohio State University, Columbus.

Uman, M. A.: 1969, *Lightning*, McGraw-Hill, New York.

Wallace, L. and Hunten, D. M.: 1978, 'The Jovian Spectrum in the Region 0.4–1.1 μm: The C/H Ratio', *Rev. Geophys. Space Phys.* **16**, 289.

Weidenschilling, S. J. and Lewis, J. S.: 1973, 'Atmospheric and Cloud Structure of the Jovian Planets', *Icarus* **20**, 465.

West, R. A.: 1979, 'Spatially Resolved Methane Band Photometry of Jupiter. II. Analysis of the South Equatorial Belt and South Tropical Zone Reflectivity', *Icarus* **38**, 34.

West, R. A. and Tomasko, M. G.: 1980, 'Spatially Resolved Methane Band Photometry of Jupiter. III. Cloud Vertical Structures for Several Axisymmetric Bands and the Great Red Spot', *Icarus* **41**, 278.

West, R. A., Hord, C., Simmons, K., Coffeen, D., Sato, M., and Lane, A.: 1981, 'Near-Ultraviolet Scattering Properties of Jupiter', *J. Geophys. Res.* **86**, 8783.

West, R. A., Kupferman, P. N., and Hart, H.: 1985, 'Voyager 1 Imaging and IRIS Observations of Jovian Methane Absorption and Thermal Emission: Implications for Cloud Structure', *Icarus* **61**, 311.

Westphal, J. A., Matthews, K., and Taylor, R. J.: 1974, 'Five Micron Pictures of Jupiter', *Astrophys. J.* **188**, L111.

Williams, G. P.: 1978, 'Planetary Circulations: 1. Barotropic Representations of Jovian and Terrestrial Turbulence', *J. Atmos. Sci.* **35**, 1399.

Williams, G. P.: 1979, 'Planetary Circulations: 2. The Jovian Quasi-Geostrophic Regime', *J. Atmos. Sci.* **36**, 932.

Williams, M. A., Krider, E. P., and Hunten, D. M.: 1983, 'Planetary Lightning: Earth, Jupiter, and Venus', *Rev. Geophys. Space Phys.* **21**, 892.

Yung, Y. L. and McElroy, M. B.: 1977, 'Stability of an Oxygen Atmosphere on Ganymede', *Icarus* **30**, 97.